Available online at www.sciencedirect.com
ScienceDirect
Comput. Methods Appl. Mech. Engrg. 395 (2022) 114963
Computer methods in applied mechanics and engineering
www.elsevier.com/locate/cma

Fully-decoupled, energy stable second-order time-accurate and finite element numerical scheme of the binary immiscible Nematic-Newtonian model

Chuanjun Chen[a], Xiaofeng Yang[b,*]

[a] School of Mathematics and Information Sciences, Yantai University, Yantai 264005, China
[b] Department of Mathematics, University of South Carolina, Columbia, SC 29208, United States of America

Received 29 December 2021; received in revised form 27 March 2022; accepted 1 April 2022
Available online xxxx

Abstract

We consider the numerical approximation of a two-phase complex fluid flow model that couples the immiscible liquid crystal fluid component immersed in the ambient free flow field, where the free interface motion between the two fluids is simulated by using the phase-field approach via the energy variational method. The model is a highly nonlinear coupling system, which is composed of the Navier–Stokes equations for the flow field, the Cahn–Hilliard equations for the free moving interface, and the constitutive equation for the nematic liquid crystal. This paper proposes an effective full-discrete finite element numerical scheme to solve the model and makes the scheme not only have the characteristics of linearity, second-order time accuracy, unconditional energy stability, decoupling structure but also only need to solve a few constant-coefficient elliptic equations at each time step. The unconditional energy stability of the scheme and the detailed implementation process are further given. Various numerical experiments including the well-known “beads-on-string" phenomena are also simulated to illustrate the effectiveness of the scheme.

Keywords: Finite element; Nematic-Newtonian; Phase-field; Energy stability; Second-order; Decoupled

1. Introduction

In this article, we consider numerical approximations of a two-phase complex fluid flow model describing the dynamic changes of liquid crystal (LC) fluid components immersed in the free flow field. The binary immiscible mixture of nematic LCs and viscous Newtonian fluid has many important technical applications, such as micro-fluidics, polymer-stabilized liquid crystal, polymer-dispersed liquid crystal, etc. The governing model is a coupling and highly nonlinear time evolution system in the form, consisting of the Navier–Stokes equations of the flow field, the Cahn–Hilliard equation of the freely moving interface, and the constitutive equation of the nematic LCs. For simplicity, we refer to this model as the phase-field nematic-Newtonian model (PF-NN, for short) in this article.

The application of the phase-field (or called diffusive interface) approach to describe the multiphase fluid flow system usually uses a scalar variable to mark the position of the interface and assumes the so-called mixing energy

* Corresponding author.
E-mail addresses: cjchen@ytu.edu.cn (C. Chen), xfyang@math.sc.edu (X. Yang).

https://doi.org/10.1016/j.cma.2022.114963
0045-7825/

to describe the hydrophilic–hydrophobic interaction of the fluid mixture. Since one of the fluid components is a nematic liquid crystal material, a part of the energy of the system also contains a potential to describe the nematic liquid crystal, which adopts Ericksen–Leslie formalism and uses a director field variable to describe the orientation of LC molecules. In addition, the model also needs an energy potential to represent the anchoring between the director field and the fluid interface along which the LC molecules have a certain orientation tendency. Finally, by coupling the kinetic energy of the flow field to the total free energy and applying the gradient flow method (e.g., Cahn–Hilliard dynamics for the phase-field variable and the Allen–Cahn dynamics for the nematic director field) to minimize the free energy, a governing system can be derived, in which several nonlinear equations are coupled together to form a highly nonlinear system.

The PF-NN model for simulating the multiphase complex fluid flow can be roughly divided into two categories if they are classified from the perspective of the coupling method of the phase-field variable and the LC director field, namely, the so-called "weight function" model, see [1–4], and the so-called "phase-transition" model, see [5,6]. The former model uses a weight function to simply multiply with the energy potential of LC, thereby restricting the orientation of the director field to a specific fluid component. The latter model adopts a phase transition mechanism so that in the non-LC fluid component, the director field will quickly dissipate to zero, so as to achieve the purpose of confining the director field to the LC fluid component. The two models can achieve the same effect, in the end, that is, the director field can only appear on a specific fluid component approximately, but the model obtained by the latter method is relatively simple because the dissipative term in the LC equation in the former model is multiplied by the weight function, while the same term appeared in the latter model is always constant-coefficient. Therefore, this paper considers the algorithm development of the latter model, which is the relatively simple model obtained by the phase transition method.

However, because the PF-NN model has a complex coupling structure and involves a large number of nonlinear terms (e.g. the advection, surface tension, the frame invariant derivative, etc.), it is very challenging to design an effective and easy-to-implement numerical scheme for the model. In addition, if it is desired to establish a high-standard scheme with many expected characteristics, such as a linear and energy stable numerical scheme with second-order time accuracy and decoupled computation, the difficulty will become even greater. For simplicity, we refer to numerical schemes with these characteristics as "ideal" types. The existence of many nonlinear coupling terms in this model hinders the design of such "ideal" type numerical schemes. These terms, including (i) advection and surface tension terms, and (ii) the frame invariant time derivative and viscous stress from the director-field of LCs [6–14], make the velocity field, director field and phase-field variables inseparably coupled together, so it is difficult to obtain an ideal type scheme. To the best of the author's knowledge, we do not yet know that any "ideal" type of schemes for the PF-NN model exist. For example, the scheme constructed in [6,12] has linear, decoupled, and energy-stable characteristics, but it is only first-order time accurate. Therefore, from a practical point of view, for the large number of nonlinear terms contained in the PF-NN model, the traditional explicit and implicit methods or their combination processing methods are difficult to achieve our goal of constructing the "ideal" type numerical schemes. Hence, more effective numerical tools need to be invented.

In this article, by extending the idea of "zero-energy-contribution" introduced in [15–19] which has been used to design a decoupling scheme for a relatively simple coupling model of the two-phase Newtonian fluid flow (both fluid components are Newtonian), we achieve the goal, namely, a fully discrete numerical scheme with the required desirable properties (linearity, decoupling, temporal second-order accuracy, energy stability, etc.) for the PF-NN model is established in this article. We need to emphasize that this extension is non-trivial compared to the work in [15] for the two-phase Newtonian model. This is because that the method given in [15] can only effectively deal with the direct coupling between the advection term in the Cahn–Hilliard equation and the surface tension term in the fluid equation, thereby obtaining a decoupled linear and second-order time accurate scheme. However, as mentioned earlier, the complexity of the coupling terms included in the PF-NN model studied in this article far exceeds the complexity of the two-phase Newtonian fluid model studied in [15], such as the coupling of the LC director field, the fluid velocity, as well as the phase-field variable, etc. It is unclear whether the idea of "zero-energy-contribution" idea of dealing with simple models in [15] can be extended to the PF-NN model studied in this article. Moreover, the numerical scheme in [15] is only semi-discrete in time, that is, the space is assumed to be continuous without being discretized, while the numerical scheme designed in this article is a fully-discrete version, which is significantly different from the work in [15].

We now briefly describe how to construct the newly developed scheme in this article. The key idea of the time advancement strategy of the scheme is to introduce two extra auxiliary variables (one is nonlocal and the other

is local) and design some ordinary differential equations (ODEs) for them. The local variable helps to rewrite the nonlinear energy potential as a quadratic function to facilitate linearization, and the nonlocal variable helps to decouple the coupled nonlinear terms. By combining with these variable and ODEs, the original system is reconstructed into another equivalent form. When designing the numerical scheme, we discretize the equivalent modified model instead of the original model. Its advantage is that the unconditional energy stability can be easily obtained by using a simple explicit method to discretize the nonlinear terms. Moreover, the introduced nonlocal variable can also help decompose each discrete equation into several constant-coefficient sub-equations. In this way, at each time step, each split variable can be solved completely independently, thereby greatly improving the calculation efficiency.

By combining this novel time marching strategy, the projection method for the fluid equations, and the finite element method for spatial discretization, a fully discrete scheme with all characteristics of the "ideal" type mentioned above is finally achieved. The solvability and the unconditional energy stability of the proposed scheme have been rigorously proven, and several numerical examples such as the so-called "beads-on-string" phenomenon of complex fluids have been simulated to further prove the effectiveness of the scheme. As far as the author knows, for the PF-NN model, the scheme developed in this article can be regarded as the first fully discrete scheme that can simultaneously have linearity, decoupling, second-order time accuracy, and unconditional energy stability, namely, the desired "ideal" type properties.

The article is organized as follows. In Section 2, the PF-NN model is briefly introduced and its law of energy dissipation is verified. In Section 3, we construct a fully discrete scheme of "ideal" type and describe its implementations in detail. Unconditional energy stability and solvability are also proved rigorously. In Section 4, we perform several accuracy/stability tests and implement various simulations to demonstrate the effectiveness of the scheme. In Section 5, some concluding remarks are given finally.

2. Model system

Here are some notations that will be used in the rest of this article. The computed domain $\Omega \in \mathbb{R}^d, d = 2, 3$ is assumed to be open, rectangular, smooth and bounded. For any two functions $\phi(\boldsymbol{x})$ and $\psi(\boldsymbol{x})$, their L^2-inner product on Ω is denoted by $(\phi, \psi) = \int_\Omega \phi(\boldsymbol{x})\psi(\boldsymbol{x})d\boldsymbol{x}$, and the L^2-norm of $\phi(\boldsymbol{x})$ is denoted by $\|\phi\| = (\phi, \phi)^{\frac{1}{2}}$.

Now, we give a brief introduction of the PF-NN model, see also in [1,5,6,20]. To model an immiscible mixture of nematic LC fluids immersed in a viscous fluid matrix, we introduce a phase-field variable $\phi(\boldsymbol{x}, t)$ as a labeling function defined as

$$\phi(\boldsymbol{x}, t) = \begin{cases} 1, & \text{nematic LC fluid,} \\ 0, & \text{Newtonian viscous fluid.} \end{cases} \tag{2.1}$$

We also introduce a unit director field variable $\mathbf{d}$ ($|\mathbf{d}| = 1$) to denote the director field representing the orientation of the LC molecules. The interface between nematic LC fluid and the Newtonian viscous fluid is described by the level set $\{\boldsymbol{x} : \phi(\boldsymbol{x}, t) = \frac{1}{2}\}$.

As mentioned in the introduction, the free energy of the PF-NN system includes three parts which are described below.

First, to represent the hydrophobic–hydrophilic tendency of two fluid components, a well-known mixing energy for the binary fluid mixture in the phase-field framework reads as

$$E_{mix}(\phi) = \int_\Omega \Big(\frac{\lambda}{2}|\nabla\phi|^2 + F(\phi)\Big)d\boldsymbol{x}, \tag{2.2}$$

where λ is associated with the binary fluid interfacial tension, $F(\phi)$ is the double-well potential that reads as $F(\phi) = \frac{1}{4\epsilon^2}\phi^2(1-\phi)^2$ with ϵ as the thickness of the transitional layer. It can be seen that $F(\phi)$ takes $\phi = 0$ and $\phi = 1$ as two bulk values. The gradient term represents the conformational entropy, promoting material mixing, while the double-well bulk energy density represents the hydrophobic interaction, promoting the phase separation of the two fluid components.

Second, the Oseen-Frank distortional elastic energy formulation E_{ela} with one Frank elastic constant approximation ($K_1 = K_2 = K_3 = K$, cf. [6,12–14,21–23]) is adopted to represent the elastic energy for the nematic LC phase, that reads as

$$E_{ela}(\mathbf{d}) = \int_\Omega \left(\frac{K}{2}|\nabla\mathbf{d}|^2 + \frac{\alpha}{4}|\mathbf{d}|^4 - \frac{\alpha}{2}\frac{\phi-\phi_c}{\phi_c}|\mathbf{d}|^2\right)d\boldsymbol{x}, \tag{2.3}$$

where $\phi_c = \frac{1}{2}$, and α is the penalizing parameter. The term $\frac{\phi-\phi_c}{\phi_c}$ is the so-called "phase transition" technique (cf. [5,6]), which is used to restrict the elastic energy only on the LC phase. When $\phi = 1$ (nematic phase), the nonlinear bulk potential in (2.3) becomes $\frac{\alpha}{4}(|\mathbf{d}|^2-1)^2 - \frac{\alpha}{4}$ that implies $|\mathbf{d}| \to 1$ for minimization; when $\phi = 0$ (viscous phase), the bulk potential becomes $\frac{\alpha}{4}(|\mathbf{d}|^4 + |\mathbf{d}|^2)$ that implies $|\mathbf{d}| \to 0$ for minimization.

Third, to accommodate both the parallel and normal anchoring of nematic LC along the fluid interface, E_{anch} is used for the anchoring energy (cf. [1,5,6,20]), that reads as

$$E_{anch}(\mathbf{d},\phi) = \int_\Omega \eta\Big(\frac{\gamma}{2}(\mathbf{d}\cdot\nabla\phi)^2 + \frac{1-\gamma}{2}\big(|\mathbf{d}|^2|\nabla\phi|^2 - (\mathbf{d}\cdot\nabla\phi)^2\big)\Big)d\boldsymbol{x}, \tag{2.4}$$

where $\eta > 0$ controls the strength of the anchoring potential. The parameter γ only takes two different values, when $\gamma = 1$ is for parallel anchoring, and $\gamma = 0$ is for normal anchoring, respectively.

The total energy of the system is the summation of the above three parts, that reads as follows,

$$E(\mathbf{d},\phi) = E_{mix}(\phi) + E_{ela}(\mathbf{d},\phi) + E_{anch}(\mathbf{d},\phi). \tag{2.5}$$

Therefore, the PF-NN model (cf. [1,5,6,20]) reads as:

$$\mathbf{d}_t + \mathbf{u}\cdot\nabla\mathbf{d} + \frac{1-s}{2}\mathbf{d}\nabla\mathbf{u} - \frac{1+s}{2}\mathbf{d}\cdot\nabla\mathbf{u} = -M_1\boldsymbol{\omega}, \tag{2.6}$$

$$\boldsymbol{\omega} = -K\Delta\mathbf{d} + \alpha(\mathbf{d}\cdot\mathbf{d})\mathbf{d} - \alpha\frac{\phi-\phi_c}{\phi_c}\mathbf{d} + \mathbf{W}_\mathbf{d}, \tag{2.7}$$

$$\phi_t + \nabla\cdot(\phi\mathbf{u}) = M_2\Delta\mu, \tag{2.8}$$

$$\mu = -\lambda\Delta\phi + f(\phi) - \frac{\alpha}{2\phi_c}\mathbf{d}\cdot\mathbf{d} + W_\phi, \tag{2.9}$$

$$\mathbf{u}_t + (\mathbf{u}\cdot\nabla)\mathbf{u} - \nu\Delta\mathbf{u} + \nabla p = \boldsymbol{\omega}\nabla\mathbf{d} - \phi\nabla\mu + \nabla\cdot\sigma_e, \tag{2.10}$$

$$\nabla\cdot\mathbf{u} = 0, \tag{2.11}$$

where

$$f(\phi) = F'(\phi) = \frac{1}{\epsilon^2}\phi(\phi-\frac{1}{2})(\phi-1),\ \boldsymbol{\omega} = \frac{\delta E(\mathbf{d},\phi)}{\delta\mathbf{d}},\ \mu = \frac{\delta E(\mathbf{d},\phi)}{\delta\phi},$$

$$\mathbf{W}_\mathbf{d} = \frac{\delta E_{anch}(\mathbf{d},\phi)}{\delta\mathbf{d}} = \eta\gamma(\mathbf{d}\cdot\nabla\phi)\nabla\phi + \eta(1-\gamma)(|\nabla\phi|^2\mathbf{d} - (\mathbf{d}\cdot\nabla\phi)\nabla\phi),$$

$$W_\phi = \frac{\delta E_{anch}(\mathbf{d},\phi)}{\delta\phi} = -\eta\gamma\nabla\cdot((\mathbf{d}\cdot\nabla\phi)\mathbf{d}) + \eta(1-\gamma)\big(\nabla\cdot((\mathbf{d}\cdot\nabla\phi)\mathbf{d}) - \nabla\cdot(|\mathbf{d}|^2\nabla\phi)\big),$$

$$\sigma_e = -\frac{1-s}{2}\mathbf{d}\boldsymbol{\omega} + \frac{1+s}{2}\boldsymbol{\omega}\mathbf{d},$$

s is a geometry parameter of the liquid crystal molecule [6,24], $\mathbf{u}$ is the fluid velocity, τ is a positive parameter, M_1, M_2 are two positive mobility parameters. p is the pressure, σ_e is the elastic stress tensor due to liquid crystal molecules [1,6,13,14,24–26]. The tensor products are defined as $\mathbf{d}\nabla\mathbf{u} := (\nabla\mathbf{u})^T\mathbf{d}$ and $\mathbf{d}\cdot\nabla\mathbf{u} := \nabla\mathbf{u}\cdot\mathbf{d}$. Here, the two fluid components are assumed to have matching viscosity ν for simplicity.

We consider the following boundary conditions, that read as

$$\mathbf{u}|_{\partial\Omega} = \mathbf{0},\ \partial_\mathbf{n}\phi|_{\partial\Omega} = \partial_\mathbf{n}\mu|_{\partial\Omega} = 0,\ \partial_\mathbf{n}\mathbf{d}|_{\partial\Omega} = \mathbf{0}, \tag{2.12}$$

where $\mathbf{n}$ is the outward normal on the boundary. The initial conditions read as,

$$(\mathbf{u}, p, \phi, \mathbf{d})|_{t=0} = (\mathbf{u}^0, p^0, \phi^0, \mathbf{d}^0). \tag{2.13}$$

Remark 2.1. We briefly explain the model (2.6)–(2.11). The equations for $\mathbf{d}$ ((2.6)–(2.7)) and ϕ ((2.8)–(2.9)) are derived by taking the variational gradient flow approach for the total free energy in the L^2 and H^{-1}, respectively. The three nonlinear terms of the invariant time derivative of the director field $\mathbf{u}\cdot\nabla\mathbf{d} + \frac{1-s}{2}\mathbf{d}\nabla\mathbf{u} - \frac{1+s}{2}\mathbf{d}\cdot\nabla\mathbf{u}$ in many works, cf. [6,13,14,25,26]), are written as an equivalent form of $\mathbf{u}\cdot\nabla\mathbf{d} - \boldsymbol{W}\cdot\mathbf{d} - s\boldsymbol{D}\cdot\mathbf{d}$ where $\boldsymbol{W} = \frac{1}{2}(\nabla\mathbf{u} - (\nabla\mathbf{u})^T)$ is the vorticity tensor, and $\boldsymbol{D} = \frac{1}{2}(\nabla\mathbf{u} + (\nabla\mathbf{u})^T)$ is the rate of strain tensor. The time derivatives of any internal variables in continuum mechanics follow the frame indifferent or invariant concerning translation and rigid body rotation. Consequently, the invariant time derivative of the director vector $\mathbf{d}$ contains three parts

- part I: the part of material derivative transporting the center of mass: $\mathbf{d}_t + \mathbf{u}\cdot\nabla\mathbf{d}$;
- part II: the part rotating the director field due to the fluid vorticity: $-\boldsymbol{W}\cdot\mathbf{d}$;
- part III: the flow-induced kinematic change of stretching or compressing of the liquid crystal molecules: $-s\boldsymbol{D}\cdot\mathbf{d}$ (for a flexible/extensible molecule) or $-s\boldsymbol{D}\cdot\mathbf{d} + s\boldsymbol{D} : \mathbf{ddd}$ (for rigid molecule).

Since the nonlinear terms (part I-III) related to the invariant time derivative and the viscous stress σ_e couple the director field and the velocity field, as far as the author knows, almost all numerical analysis are based on the simplified version, that is, only the material derivative in part I is considered, while the terms of part II-III and the stress σ_e are usually neglected due to their highly coupled and nonlinear structure. In our previous work [6,13,14], we have attempted to construct numerical schemes for the fluid flow coupled with the director field model, however, the obtained numerical schemes only have first-order time accuracy or nonlinear structure, although they have provable energy stability.

The PF-NN model (2.6)–(2.11) follows the law of energy dissipation, which is shown in the following Lemma.

Lemma 2.1. *The following energy law holds for the PF-NN system (2.6)–(2.11):*

$$\frac{d}{dt}E_{tot}(\phi,\mathbf{d},\mathbf{u}) = -M_1\|\boldsymbol{\omega}\|^2 - M_2\|\nabla\mu\|^2 - \nu\|\nabla\mathbf{u}\|^2, \tag{2.14}$$

where

$$E_{tot}(\phi,\mathbf{d},\mathbf{u}) = E(\phi,\mathbf{d}) + \frac{1}{2}\|\mathbf{u}\|^2. \tag{2.15}$$

Proof. First, by multiplying the inner product of (2.6) with $\boldsymbol{\omega}$ in L^2 space, we get

$$(\mathbf{d}_t,\boldsymbol{\omega}) = -M_1\|\boldsymbol{\omega}\|^2 - (\mathbf{u}\cdot\nabla\mathbf{d},\boldsymbol{\omega}) - \frac{1-s}{2}(\mathbf{d}\nabla\mathbf{u},\boldsymbol{\omega}) + \frac{1+s}{2}(\mathbf{d}\cdot\nabla\mathbf{u},\boldsymbol{\omega}). \tag{2.16}$$

We take the inner product of (2.7) with $-\mathbf{d}_t$ in the L^2 space, we get

$$-(\boldsymbol{\omega},\mathbf{d}_t) = -\left(-K\Delta\mathbf{d} + \alpha(\mathbf{d}\cdot\mathbf{d})\mathbf{d} - \alpha\frac{\phi-\phi_c}{\phi_c}\mathbf{d} + \mathbf{W}_{\mathbf{d}},\mathbf{d}_t\right) = -(\frac{\delta E}{\delta\mathbf{d}},\mathbf{d}_t). \tag{2.17}$$

By combining the above two obtained equations together and using integration by parts, we get

$$(\frac{\delta E}{\delta\mathbf{d}},\mathbf{d}_t) = -M_1\|\boldsymbol{\omega}\|^2 \underbrace{-(\mathbf{u}\cdot\nabla\mathbf{d},\boldsymbol{\omega})}_{\mathrm{I}_1} \underbrace{-\frac{1-s}{2}(\mathbf{d}\nabla\mathbf{u},\boldsymbol{\omega})}_{\mathrm{III}_1} + \underbrace{\frac{1+s}{2}(\mathbf{d}\cdot\nabla\mathbf{u},\boldsymbol{\omega})}_{\mathrm{IV}_1}. \tag{2.18}$$

Second, we take the inner product of (2.8) with μ to derive

$$(\phi_t,\mu) + (\nabla\cdot(\phi\mathbf{u}),\mu) = -M_2\|\nabla\mu\|^2. \tag{2.19}$$

We take the inner product of (2.9) with $-\phi_t$ in L^2 to get

$$-(\mu,\phi_t) = -\left(-\lambda\Delta\phi + f(\phi) - \frac{\alpha}{2\phi_c}\mathbf{d}\cdot\mathbf{d} + W_\phi,\phi_t\right) = -(\frac{\delta E}{\delta\phi},\phi_t). \tag{2.20}$$

By using integration by parts and combining the above two equations together, we get

$$(\frac{\delta E}{\delta\phi},\phi_t) = -M_2\|\nabla\mu\|^2 \underbrace{-(\nabla\cdot(\phi\mathbf{u}),\mu)}_{\mathrm{II}_1}. \tag{2.21}$$

Third, we take the inner product of (2.10) with $\mathbf{u}$ in L^2, and use (2.11) to obtain

$$\begin{aligned}\frac{d}{dt}(\frac{1}{2}\|\mathbf{u}\|^2) + \nu\|\nabla\mathbf{u}\|^2 = &\underbrace{(\boldsymbol{\omega}\nabla\mathbf{d},\mathbf{u})}_{\mathrm{I}_2} \underbrace{-(\phi\nabla\mu,\mathbf{u})}_{\mathrm{II}_2} \underbrace{-\frac{1-s}{2}(\nabla\cdot(\mathbf{d}\boldsymbol{\omega}),\mathbf{u})}_{\mathrm{III}_2} + \underbrace{\frac{1+s}{2}(\nabla\cdot(\boldsymbol{\omega}\mathbf{d}),\mathbf{u})}_{\mathrm{IV}_2}\\ &- \underbrace{((\mathbf{u}\cdot\nabla)\mathbf{u},\mathbf{u})}_{\mathrm{V}}.\end{aligned} \tag{2.22}$$

We can derive the energy law (2.14) after combining (2.18), (2.21), and (2.22) (using Remark 2.2). □

Remark 2.2. The derivation of the energy law (2.14) applies all inner product terms labeled by the same Roman numerals to be canceled out or exactly equal to zero, namely,

$$\mathrm{I}_1+\mathrm{I}_2=0,\ \mathrm{II}_1+\mathrm{II}_2=0,\ \mathrm{III}_1+\mathrm{III}_2=0,\ \mathrm{IV}_1+\mathrm{IV}_2=0, \mathrm{V}=0, \tag{2.23}$$

which can be derived by using the integration by parts and the boundary conditions for $\mathbf{u}$ (note that the last two equalities also use the two identities: $-(\mathbf{d}\nabla\mathbf{u},\boldsymbol{\omega})+(\mathbf{d}\boldsymbol{\omega},\nabla\mathbf{u})=0$, $(\mathbf{d}\cdot\nabla\mathbf{u},\boldsymbol{\omega})-(\boldsymbol{\omega}\mathbf{d},\nabla\mathbf{u})=0$).

The equations in (2.23) can be viewed as the contribution of all these nonlinear terms to the total free energy of the system is zero. This feature of "zero-contribution-energy" prompts us how to build a decoupling type scheme, see the next section.

3. Numerical scheme

From the form of the PF-NN system (2.6)–(2.11), we can see that it is very difficult to design an "ideal" type numerical scheme by using simple explicit/implicit processing of a large number of coupled nonlinear terms, including the advection, the surface tension, the frame invariant derivative, the viscous stress, the nonlinear cubic term $f(\phi)$, the phase transition term, the anchoring coupling potential, and the coupling between velocity and pressure through the divergence-free condition. To design special numerical techniques to realize the linearization and decouplings, instead of carefully distinguishing whether each nonlinear term is discretized using implicit or explicit methods, we introduce a new method to realize the decoupled calculation, where the key idea is to reformulate the system into an equivalent version by introducing some newly defined variables. The detailed process is given as follows.

3.1. Reformulated equivalent system and energy law

Now, by introducing some auxiliary variables, we reconstruct the original governing system into a different but equivalent form, which can provide great convenience for designing easy-to-implement and decoupling-type schemes.

We first define an auxiliary variable $U(\boldsymbol{x},t)$ of local type, which plays a key role to linearize the nonlinear terms. $U(\boldsymbol{x},t)$ reads as

$$U=\sqrt{N(\phi,\mathbf{d})+B}, \tag{3.1}$$

where

$$\begin{aligned} N(\phi,\mathbf{d}) &= F(\phi)+\frac{\alpha}{4}|\mathbf{d}|^4-\frac{\alpha}{2}\frac{\phi-\phi_c}{\phi_c}|\mathbf{d}|^2-\frac{S_\phi}{2}\phi^2-\frac{S_\mathbf{d}}{2}|\mathbf{d}|^2 \\ &\quad+\eta\Big(\frac{\gamma}{2}(\mathbf{d}\cdot\nabla\phi)^2+\frac{1-\gamma}{2}\big(|\mathbf{d}|^2|\nabla\phi|^2-(\mathbf{d}\cdot\nabla\phi)^2\big)\Big), \end{aligned} \tag{3.2}$$

B, S_ϕ, $S_\mathbf{d}$ are three positive constants. Note that $F(\phi)$ is a fourth-order polynomial term with a positive leading order term, thus it surely bounds the quadratic term $-\frac{S_\phi}{2}\phi^2$ from below for any constant S_ϕ. Similarly, the negative $-\frac{S_\mathbf{d}}{2}|\mathbf{d}|^2$ is bounded from below by the fourth order term $|\mathbf{d}|^4$. Therefore, it can be guaranteed that $N(\phi,\mathbf{d})$ is always bounded from below (the lower bound is up to the constants $S_\mathbf{d}$ and S_ϕ). To further ensure the radicand positive, we add a positive constant B in the square root.

Using the variable U, we rewrite (2.7) and (2.9) as follows:

$$\boldsymbol{\omega}=-K\Delta\mathbf{d}+S_\mathbf{d}\mathbf{d}+\underbrace{\mathbf{H}U}_{\mathrm{U-reform}}, \tag{3.3}$$

$$\mu=-\lambda\Delta\phi+S_\phi\phi+\underbrace{RU}_{\mathrm{U-reform}}, \tag{3.4}$$

$$U_t=\frac{1}{2}\mathbf{H}\cdot\mathbf{d}_t+\frac{1}{2}R\phi_t, \tag{3.5}$$

where $U|_{t=0}=\sqrt{N(\phi^0,\mathbf{d}^0)+B}$, (3.5) is obtained by taking the derivative of U defined in (3.1), and

$$\mathbf{H}=\frac{\alpha(\mathbf{d}\cdot\mathbf{d})\mathbf{d}-\alpha\frac{\phi-\phi_c}{\phi_c}\mathbf{d}+\mathbf{W}_\mathbf{d}-S_\mathbf{d}\mathbf{d}}{\sqrt{N(\phi,\mathbf{d})+B}},\quad R=\frac{f(\phi)-\frac{\alpha}{2\phi_c}\mathbf{d}\cdot\mathbf{d}+W_\phi-S_\phi\phi}{\sqrt{N(\phi,\mathbf{d})+B}}.$$

Note that the newly defined variable U is used to reformulate the terms above the brackets, so we use "U-reform" to mark them in the above equations. The equivalence between the newly obtained Eqs. (3.3)–(3.4)–(3.5) and (2.7)–(2.9) is straightforward, which can be shown by performing a simple integration of (3.5) together with the initial condition of U that can recover (3.1), therefore (2.7) and (2.9) are obtained by using (3.3) and (3.4).

Second, we introduce a trivial nonlocal variable $Q(t)$ and design a trivial ODE system for it. They will plays a critical role to realize the decoupling structure of the numerical scheme. $Q(t)$ and its ODE read as:

$$\begin{cases} Q_t = ((\mathbf{u}\cdot\nabla)\mathbf{u},\mathbf{u}) + (\mathbf{u}\cdot\nabla\mathbf{d},\boldsymbol{\omega}) - (\boldsymbol{\omega}\nabla\mathbf{d},\mathbf{u}) + (\nabla\cdot(\phi\mathbf{u}),\mu) + (\phi\nabla\mu,\mathbf{u}) \\ \qquad\quad + \dfrac{1-s}{2}(\mathbf{d}\nabla\mathbf{u},\boldsymbol{\omega}) + \dfrac{1-s}{2}(\nabla\cdot(\mathbf{d}\boldsymbol{\omega}),\mathbf{u}) \\ \qquad\quad - \dfrac{1+s}{2}(\mathbf{d}\cdot\nabla\mathbf{u},\boldsymbol{\omega}) - \dfrac{1+s}{2}(\nabla\cdot(\boldsymbol{\omega}\mathbf{d}),\mathbf{u}) \\ \qquad\quad - (\mathbf{H}\cdot\mathbf{d}_t,U) + (\mathbf{H}U,\mathbf{d}_t) - (R\phi_t,U) + (RU,\phi_t), \\ Q|_{(t=0)} = 1, \end{cases} \tag{3.6}$$

where $\mathbf{u}$ satisfies the boundary conditions given in (2.12). From Remark 2.2, we note that the ODE (3.6) is exactly the same as the trivial ODE: $Q_t = 0$, $Q|_{t=0} = 1$ which has $Q(t) = 1$ as the exact solution.

Third, using the two new variables, the local variable $Q(t)$ and the nonlocal variable $U(\boldsymbol{x},t)$, and by combining equations of ((3.3), (3.4), (3.5)), Eq. (3.6), and equations of ((2.6), (2.8), (2.10), (2.11)), we rewrite the original system (2.6)–(2.11) into the following form:

$$\mathbf{d}_t + \underbrace{Q\left(\mathbf{u}\cdot\nabla\mathbf{d} + \frac{1-s}{2}\mathbf{d}\nabla\mathbf{u} - \frac{1+s}{2}\mathbf{d}\cdot\nabla\mathbf{u}\right)}_{\text{Q-reform}} = -M_1\boldsymbol{\omega}, \tag{3.7}$$

$$\boldsymbol{\omega} = -K\Delta\mathbf{d} + S_{\mathbf{d}}\mathbf{d} + \underbrace{Q\mathbf{H}U}_{\text{Q-reform}}, \tag{3.8}$$

$$\phi_t + \underbrace{Q\nabla\cdot(\phi\mathbf{u})}_{\text{Q-reform}} = M_2\Delta\mu, \tag{3.9}$$

$$\mu = -\lambda\Delta\phi + S_\phi\phi + \underbrace{QRU}_{\text{Q-reform}}, \tag{3.10}$$

$$U_t = \underbrace{Q\left(\frac{1}{2}\mathbf{H}\cdot\mathbf{d}_t + \frac{1}{2}R\phi_t\right)}_{\text{Q-reform}}, \tag{3.11}$$

$$\mathbf{u}_t + \underbrace{Q(\mathbf{u}\cdot\nabla)\mathbf{u}}_{\text{Q-reform}} - \nu\Delta\mathbf{u} + \nabla p = \underbrace{Q\left(\boldsymbol{\omega}\nabla\mathbf{d} - \phi\nabla\mu - \frac{1-s}{2}\nabla\cdot(\mathbf{d}\boldsymbol{\omega}) + \frac{1+s}{2}\nabla\cdot(\boldsymbol{\omega}\mathbf{d})\right)}_{\text{Q-reform}}, \tag{3.12}$$

$$\nabla\cdot\mathbf{u} = 0, \tag{3.13}$$

$$\begin{aligned} Q_t = {} & ((\mathbf{u}\cdot\nabla)\mathbf{u},\mathbf{u}) + (\mathbf{u}\cdot\nabla\mathbf{d},\boldsymbol{\omega}) - (\boldsymbol{\omega}\nabla\mathbf{d},\mathbf{u}) + (\nabla\cdot(\mathbf{u}\phi),\mu) + (\phi\nabla\mu,\mathbf{u}) \\ & + \frac{1-s}{2}(\mathbf{d}\nabla\mathbf{u},\boldsymbol{\omega}) + \frac{1-s}{2}(\nabla\cdot(\mathbf{d}\boldsymbol{\omega}),\mathbf{u}) \\ & - \frac{1+s}{2}(\mathbf{d}\cdot\nabla\mathbf{u},\boldsymbol{\omega}) - \frac{1+s}{2}(\nabla\cdot(\boldsymbol{\omega}\mathbf{d}),\mathbf{u}) \\ & - (\mathbf{H}\cdot\mathbf{d}_t,U) + (\mathbf{H}U,\mathbf{d}_t) - (R\phi_t,U) + (RU,\phi_t), \end{aligned} \tag{3.14}$$

where we note that in the new modified system (3.7)–(3.14), those terms involved in Remark 2.2 are all multiplied by the new nonlocal variable Q. The reason for performing such a modification of the original equation is that the solution of ODE (3.14) is $Q(t) = 1$, so the PDE system has not been changed by this modification.

The following initial conditions are satisfied by the transformed system (3.7)–(3.14), that is,

$$(\mathbf{u},\, p,\, \phi,\, \mathbf{d})|_{t=0} = (\mathbf{u}^0,\, p^0,\, \phi^0,\, \mathbf{d}^0),\; Q|_{t=0} = 1,\; U|_{t=0} = \sqrt{N(\phi^0, \mathbf{d}^0) + B}. \tag{3.15}$$

The derivation of obtaining the law of energy dissipation for the two models, (2.6)–(2.11) and (3.7)–(3.14) is slightly different although they are equivalent. Because the derivation of the latter has a guiding effect on the derivation of the energy law for the discrete scheme. Here we explain in detail how the reconstructed equivalent system maintains the energy dissipation law which is shown below.

Lemma 3.1. *The reformulated system (3.7)–(3.14) follows the energy dissipative law that reads as*

$$\frac{d}{dt}\hat{E}_{tot}(\phi, \mathbf{d}, \mathbf{u}, Q, U) = -M_1\|\boldsymbol{\omega}\|^2 - M_2\|\nabla\mu\|^2 - \nu\|\nabla\mathbf{u}\|^2, \tag{3.16}$$

where

$$\begin{aligned}\hat{E}_{tot}(\phi, \mathbf{d}, \mathbf{u}, Q, U) = &\frac{1}{2}\|\mathbf{u}\|^2 + \frac{K}{2}\|\nabla\mathbf{d}\|^2 + \frac{S_{\mathbf{d}}}{2}\|\mathbf{d}\|^2 \\ &+ \frac{\lambda}{2}\|\nabla\phi\|^2 + \frac{S_\phi}{2}\|\phi\|^2 + \|U\|^2 + \frac{1}{2}|Q|^2 - B|\Omega| - \frac{1}{2}.\end{aligned} \tag{3.17}$$

Proof. By taking the inner product of (3.7) with $\boldsymbol{\omega}$, we get

$$(\mathbf{d}_t, \boldsymbol{\omega}) = -M_1\|\boldsymbol{\omega}\|^2 \underbrace{-Q(\mathbf{u}\cdot\nabla\mathbf{d}, \boldsymbol{\omega})}_{\mathbb{A}_1} \underbrace{-\frac{1-s}{2}Q(\mathbf{d}\nabla\mathbf{u}, \boldsymbol{\omega})}_{\mathbb{E}_1} + \underbrace{\frac{1+s}{2}Q(\mathbf{d}\cdot\nabla\mathbf{u}, \boldsymbol{\omega})}_{\mathbb{F}_1}. \tag{3.18}$$

By taking the L^2 inner product of (3.8) with $-\mathbf{d}_t$, we get

$$-(\boldsymbol{\omega}, \mathbf{d}_t) = -\frac{d}{dt}\left(\frac{K}{2}\|\nabla\mathbf{d}\|^2 + \frac{S_{\mathbf{d}}}{2}\|\mathbf{d}\|^2\right) \underbrace{-Q(\mathbf{H}U, \mathbf{d}_t)}_{\mathbb{I}_1}. \tag{3.19}$$

By taking the inner product of (3.9) with μ, we get

$$(\phi_t, \mu) = -M_2\|\nabla\mu\|^2 \underbrace{-Q(\nabla\cdot(\phi\mathbf{u}), \mu)}_{\mathbb{B}_1}. \tag{3.20}$$

By multiplying the inner product of (3.10) with $-\phi_t$ in L^2, and use integration by parts to get

$$-(\mu, \phi_t) = -\frac{d}{dt}\left(\frac{\lambda}{2}\|\nabla\phi\|^2 + \frac{S_\phi}{2}\|\phi\|^2\right) \underbrace{-Q(RU, \phi_t)}_{\mathbb{J}_1}. \tag{3.21}$$

By multiplying the L^2 inner product of (3.11) with $2U$, we obtain

$$\frac{d}{dt}\|U\|^2 = \underbrace{Q(\mathbf{H}\cdot\mathbf{d}_t, U)}_{\mathbb{K}_1} + \underbrace{Q(R\phi_t, U)}_{\mathbb{L}_1}. \tag{3.22}$$

By taking the inner product of (3.12) with $\mathbf{u}$ in L^2, and use (3.13) to obtain

$$\begin{aligned}\frac{d}{dt}\left(\frac{\|\mathbf{u}\|^2}{2}\right) + \nu\|\nabla\mathbf{u}\|^2 = &\underbrace{-Q((\mathbf{u}\cdot\nabla)\mathbf{u}, \mathbf{u})}_{\mathbb{M}_1} + \underbrace{Q(\boldsymbol{\omega}\nabla\mathbf{d}, \mathbf{u})}_{\mathbb{C}_1} \underbrace{-Q(\phi\nabla\mu, \mathbf{u})}_{\mathbb{D}_1} \\ &\underbrace{-\frac{1-s}{2}Q(\nabla\cdot(\mathbf{d}\boldsymbol{\omega}), \mathbf{u})}_{\mathbb{G}_1} + \underbrace{\frac{1+s}{2}Q(\nabla\cdot(\boldsymbol{\omega}\mathbf{d}), \mathbf{u})}_{\mathbb{H}_1}.\end{aligned} \tag{3.23}$$

By multiplying (3.14) with Q, we obtain

$$\begin{aligned}\frac{d}{dt}(\frac{1}{2}|Q|^2) =& \underbrace{Q((\mathbf{u}\cdot\nabla)\mathbf{u},\mathbf{u})}_{\mathbb{M}_2}+\underbrace{Q(\mathbf{u}\cdot\nabla\mathbf{d},\boldsymbol{\omega})}_{\mathbb{A}_2}\underbrace{-Q(\boldsymbol{\omega}\nabla\mathbf{d},\mathbf{u})}_{\mathbb{C}_2}+\underbrace{Q(\nabla\cdot(\mathbf{u}\phi))}_{\mathbb{B}_2},\mu+\underbrace{Q(\phi\nabla\mu,\mathbf{u})}_{\mathbb{D}_2}\\ &+\underbrace{\frac{1-s}{2}Q(\mathbf{d}\nabla\mathbf{u},\boldsymbol{\omega})}_{\mathbb{E}_2}+\underbrace{\frac{1-s}{2}Q(\nabla\cdot(\mathbf{d}\boldsymbol{\omega}),\mathbf{u})}_{\mathbb{G}_2}\\ &\underbrace{-\frac{1+s}{2}Q(\mathbf{d}\cdot\nabla\mathbf{u},\boldsymbol{\omega})}_{\mathbb{F}_2}\underbrace{-\frac{1+s}{2}Q(\nabla\cdot(\boldsymbol{\omega}\mathbf{d}),\mathbf{u})}_{\mathbb{H}_2}\\ &\underbrace{-Q(\mathbf{H}\cdot\mathbf{d}_t,U)}_{\mathbb{K}_2}+\underbrace{Q(\mathbf{H}U,\mathbf{d}_t)}_{\mathbb{I}_2}\underbrace{-Q(R\phi_t,U)}_{\mathbb{L}_2}+\underbrace{Q(RU,\phi_t)}_{\mathbb{J}_2}.\end{aligned} \tag{3.24}$$

After combining (3.18)–(3.24), the law of energy dissipation (3.16) is obtained, because all the terms underbraced with the same letter are canceled. □

Now, through the following remarks, we explain in detail why we use the newly defined variables U and Q to transform the PDE system (2.6)–(2.11) into the new system of (3.7)–(3.14). We will answer the following four questions one by one:

- question I: why we use U to rewrite the nonlinear potential $\boldsymbol{\omega}$ and μ instead of discretizing the nonlinear terms directly;
- question II: why we create the trivial ODE for Q;
- question III: why we multiply the trivial nonlocal variable Q to many nonlinear terms instead of keeping their original form;
- question IV: why extract two quadratic terms $\frac{S_\phi}{2}\phi^2$ and $\frac{S_\mathbf{d}}{2}|\mathbf{d}|^2$ from $N(\phi,\mathbf{d})$ and define U as a square root term as (3.1).

Remark 3.1. The following remark is a comment on question I. In simple words, the aim of rewriting the chemical potentials $\boldsymbol{\omega}$ and μ is to obtain a linear and energy stable scheme. The difference between the equations of $\boldsymbol{\omega}$ and μ in the original form (2.7)–(2.9) and the new modified form (3.3)–(3.4) can fully explain why we reformulate $\boldsymbol{\omega}$ and μ in terms of the new variable U.

In the original Eqs. (2.7)–(2.9), there exists a large number of complicated nonlinear terms, and it is well known that the simple implicit or explicit discretion method will not obtain unconditionally energy stable schemes, see [27,28]. After adopting the new variable U, the nonlinear terms in (2.7) and (2.9) are transformed into a simple form, $\mathbf{H}U$ and RU. Thus one only needs to discretize them by using the semi-explicit way, that can achieve a linear and energy stable scheme. Moreover, after rewriting $\mathbf{H}U$ and RU into $Q\mathbf{H}U$ and QRU using the new nonlocal variable Q, one can even discretize these terms by using the explicit way, that can not only achieve the linear and energy stable scheme, but also the fully-decoupled structure, which also gives us some partial reason about Question III.

Remark 3.2. The following remark is a comment on questions II and III. In simple words, the aim of defining the ODE (3.14) for Q and multiplying so many nonlinear terms using Q is to obtain a full decoupling type scheme. The difference of process in obtaining the energy dissipation law between Lemmas 2.1 and 3.1 fully explains why the original system (2.6)–(2.11) is converted to an equivalent and new form (3.7)–(3.14) by using the new variable Q, which will be explained in detail by taking the advection term $\nabla\cdot(\phi\mathbf{u})$ in (2.8) as an example.

In Lemma 2.1, when deriving the energy law for the original PDE system (2.6)–(2.11), it is worthy to note that the term I_1 in (2.18) and I_2 in (2.22) are canceled. This means that the discretization of these two terms must be matched in some way, which inevitably leads to a coupling type scheme. While for the modified system (3.7)–(3.14), the term $\mathbb{B}_2$ in (3.24) can cancel $\mathbb{B}_1$, and the term $\mathbb{D}_2$ in (3.24) can cancel $\mathbb{D}_1$. This means that the term $\mathbb{B}_1$ in (3.20) and $\mathbb{D}_1$ in (3.23) do not need to cancel each other out. In other words, when developing numerical schemes, we can use different discretization methods to deal with the term $Q\nabla\cdot(\phi\mathbf{u})$ in (3.9) and the term $-Q\phi\nabla\mu$ in (3.12), thereby making it possible for constructing a complete decoupled type scheme.

Remark 3.3. The following remark is a comment on question IV. In simple words, the aim of extracting two quadratic terms is to maintain the H^1-stability of ϕ and $\mathbf{d}$, which can be seen by comparing the format of the original energy (2.15) and the modified energy (3.17).

From the format of the original energy (2.15), we see that the H^1-stability of ϕ and $\mathbf{d}$ is guaranteed, because the L^2 norm of ϕ and $\mathbf{d}$ are always bounded by the L^4 norm, which is included in the terms $F(\phi)$ and $|\mathbf{d}|^4$, respectively. After we extract two stabilization terms (S_ϕ and $S_{\mathbf{d}}$) from the nonlinear potential $N(\phi, \mathbf{d})$, the existence of these two stabilization terms, together with the gradient potential of $\|\nabla\phi\|^2$ and $\|\nabla\mathbf{d}\|^2$, can guarantee the H^1 stability of ϕ and $\mathbf{d}$ in the modified energy (3.17). In other words, if $S_\phi = S_{\mathbf{d}} = 0$, the H^1-stability of ϕ and $\mathbf{d}$ cannot be guaranteed, which will cause the practical calculation to be unstable when using a larger time step. Moreover, from the L^2 norm of ϕ in the original energy (2.15), we can see that its scale is approximately $1/\epsilon^2$. Therefore, in the modified energy, the size of the L^2 norm induced by the stabilizer S_ϕ, i.e., $\frac{S_\phi}{2}\|\phi\|^2$, should also be at the same scale. That is, $S_\phi \sim O(1/\epsilon^2)$. In the same way, it can be seen that $S_{\mathbf{d}} \sim O(\alpha)$.

Similar linear stabilization techniques have been widely used to constructing schemes for solving other gradient flow type models, e.g., the methods of IEQ, SAV, convex-splitting methods, etc., see [28–31].

Remark 3.4. Note that we add the constant $-B|\Omega| - \frac{1}{2}$ to the above modified energy (3.17), so that it is consistent with the original energy (2.15) in the continuous case. This is because in the continuous case, we have (3.1) and $Q(t) = 1$. Therefore, after adding the constant $-B|\Omega| - \frac{1}{2}$, the energy (3.17) retains the original energy (2.15), of course, in the continuous case.

3.2. Numerical scheme

We are now ready to develop the "ideal" type time marching numerical scheme for the PF-NN model. We denote the time step size by $\delta t > 0$ and set $t^n = n\delta t$ for $0 \le n \le N$ with $T = N\delta t$. Let ψ^n be the numerical approximation to the analytic function $\psi(\cdot, t)|_{t=t^n}$.

In the previous subsection, we have shown that the new modified system (3.7)–(3.14) and the original system (2.6)–(2.11) are completely equivalent. Hence, instead of considering the original system (2.6)–(2.11), we turn our attention to construct a numerical scheme for the modified system (3.7)–(3.14). This is because, in the modified model, the use of new variables provides good preparation for the linearization of the nonlinear term. The unique form of the modified model allows us to perform a simple and explicit discretization of the nonlinear terms to obtain a linear and unconditionally energy stable scheme.

Before the scheme is developed, we introduce several finite dimensional discrete subspaces. We assume that the polygonal/polyhedral domain Ω is discretized by a conforming and shape regular triangulation/tetrahedron mesh $\mathcal{T}_h$ that is composed by open disjoint elements K such that $\bar{\Omega} = \bigcup_{K\in\mathcal{T}_h} \bar{K}$. We denote $\mathcal{P}_l$ as the space of polynomials of the total degree at most l, and define some finite element spaces as follows:

$$\begin{aligned} Y_h &= \left\{X \in C^0(\Omega) : X|_K \in \mathcal{P}_{l_1}(K), \forall K \in \mathcal{T}_h\right\}, \\ \boldsymbol{V}_h &= \left\{\boldsymbol{v} \in C^0(\Omega)^d : \boldsymbol{v}|_K \in \mathcal{P}_{l_2}(K)^d, \forall K \in \mathcal{T}_h\right\} \cap H_0^1(\Omega)^d, \\ O_h &= \left\{q \in C^0(\Omega) : q|_K \in \mathcal{P}_{l_2-1}(K), \forall K \in \mathcal{T}_h\right\} \cap L_0^2(\Omega), \\ X_h &= \left\{U \in C^0(\Omega) : U|_K \in \mathcal{P}_{l_3}(K), \forall K \in \mathcal{T}_h\right\}, \end{aligned} \tag{3.25}$$

where $H_0^1(\Omega) = \{u \in H^1(\Omega) : u|_{\partial\Omega} = 0\}$ and $L_0^2(\Omega) = \{q \in L^2(\Omega) : \int_\Omega q d\boldsymbol{x} = 0\}$. Hence,

$$Y_h \subset H^1(\Omega), \boldsymbol{V}_h \subset H_0^1(\Omega)^d, O_h \subset L_0^2(\Omega), X_h \subset L^2(\Omega). \tag{3.26}$$

Besides, we assume the pair of spaces $(\boldsymbol{V}_h, O_h)$ satisfy the *inf–sup* condition [32]:

$$\beta\|q\| \le \sup_{\boldsymbol{v}\in\boldsymbol{V}_h} \frac{(\nabla\cdot\boldsymbol{v}, q)}{\|\nabla\boldsymbol{v}\|}, \quad \forall q \in O_h,$$

where the constant β only depends on Ω. A well-known *inf–sup* stable pair $(\boldsymbol{V}_h, O_h)$ is the Taylor–Hood element [32].

The semi-discrete formulation of the system (3.7)–(3.14) reads as: find $\mathbf{d} \in Y_h^d$, $\boldsymbol{\omega} \in Y_h^d$, $\phi \in Y_h$, $\mu \in Y_h$, $\mathbf{u} \in \boldsymbol{V}_h$, $p \in O_h$, $U \in X_h$, $Q \in \mathbb{R}$, such that

$$(\mathbf{d}_t, \boldsymbol{m}) + Q(\mathbf{u}\cdot\nabla\mathbf{d} + \frac{1-s}{2}\mathbf{d}\nabla\mathbf{u} - \frac{1+s}{2}\mathbf{d}\cdot\nabla\mathbf{u}, \boldsymbol{m}) = -M_1(\boldsymbol{\omega}, \boldsymbol{m}), \tag{3.27}$$

$$(\boldsymbol{\omega}, \boldsymbol{c}) = K(\nabla \mathbf{d}, \nabla \boldsymbol{c}) + S_{\mathbf{d}}(\mathbf{d}, \boldsymbol{c}) + Q(\mathbf{H}U, \boldsymbol{c}), \tag{3.28}$$

$$(\phi_t, \varpi) + Q(\nabla \cdot (\phi \mathbf{u}), \varpi) = -M_2(\nabla \mu, \nabla \varpi), \tag{3.29}$$

$$(\mu, \psi) = \lambda(\nabla \phi, \nabla \psi) + S_{\phi}(\phi, \psi) + Q(RU, \psi), \tag{3.30}$$

$$(U_t, V) = Q(\frac{1}{2}\mathbf{H} \cdot \mathbf{d}_t + \frac{1}{2} R\phi_t, V), \tag{3.31}$$

$$\begin{aligned}(\mathbf{u}_t, \mathbf{v}) + Q((\mathbf{u} \cdot \nabla)\mathbf{u}, \mathbf{v}) + \nu(\nabla \mathbf{u}, \nabla \mathbf{v}) + (\nabla p, \mathbf{v}) \\ = Q(\boldsymbol{\omega} \nabla \mathbf{d} - \phi \nabla \mu - \frac{1-s}{2} \nabla \cdot (\mathbf{d}\boldsymbol{\omega}) + \frac{1+s}{2} \nabla \cdot (\boldsymbol{\omega}\mathbf{d}), \mathbf{v}),\end{aligned} \tag{3.32}$$

$$(\nabla \cdot \mathbf{u}, q) = 0, \tag{3.33}$$

$$\begin{aligned}Q_t = &((\mathbf{u} \cdot \nabla)\mathbf{u}, \mathbf{u}) + (\mathbf{u} \cdot \nabla \mathbf{d}, \boldsymbol{\omega}) - (\boldsymbol{\omega} \nabla \mathbf{d}, \mathbf{u}) + (\nabla \cdot (\mathbf{u}\phi), \mu) + (\phi \nabla \mu, \mathbf{u}) \\ &+ \frac{1-s}{2}(\mathbf{d} \nabla \mathbf{u}, \boldsymbol{\omega}) + \frac{1-s}{2}(\nabla \cdot (\mathbf{d}\boldsymbol{\omega}), \mathbf{u}) \\ &- \frac{1+s}{2}(\mathbf{d} \cdot \nabla \mathbf{u}, \boldsymbol{\omega}) - \frac{1+s}{2}(\nabla \cdot (\boldsymbol{\omega}\mathbf{d}), \mathbf{u}) \\ &- (\mathbf{H} \cdot \mathbf{d}_t, U) + (\mathbf{H}U, \mathbf{d}_t) \\ &- (R\phi_t, U) + (RU, \phi_t),\end{aligned} \tag{3.34}$$

for $\boldsymbol{m} \in Y_h^d$, $\mathbf{c} \in Y_h^d$, $\varpi \in Y_h$, $\psi \in Y_h$, $\mathbf{v} \in \boldsymbol{V}_h$, $q \in O_h$, $V \in X_h$.

The fully discrete scheme of the system (3.7)–(3.14) reads as follows, where the second-order backward differentiation (BDF2) formula is used for the time discretization.

Find $\mathbf{d}_h^{n+1} \in Y_h^d$, $\boldsymbol{\omega}_h^{n+1} \in Y_h^d$, $\phi_h^{n+1} \in Y_h$, $\mu_h^{n+1} \in Y_h$, $\tilde{\mathbf{u}}_h^{n+1} \in \boldsymbol{V}_h$, $p_h^{n+1} \in O_h$, $U_h^{n+1} \in X_h$, and a nonlocal scalar $Q^{n+1} \in \mathbb{R}$ such that

$$\begin{aligned}(\frac{a\mathbf{d}_h^{n+1} - b\mathbf{d}_h^n + c\mathbf{d}_h^{n-1}}{2\delta t}, \boldsymbol{m}_h) = &-M_1(\boldsymbol{\omega}_h^{n+1}, \boldsymbol{m}_h) \\ &- Q^{n+1}(\mathbf{u}^* \cdot \nabla \mathbf{d}^* + \frac{1-s}{2}\mathbf{d}^* \nabla \mathbf{u}^* - \frac{1+s}{2}\mathbf{d}^* \cdot \nabla \mathbf{u}^*, \boldsymbol{m}_h),\end{aligned} \tag{3.35}$$

$$(\boldsymbol{\omega}_h^{n+1}, \boldsymbol{c}_h) = K(\nabla \mathbf{d}_h^{n+1}, \nabla \boldsymbol{c}_h) + S_{\mathbf{d}}(\mathbf{d}_h^{n+1}, \boldsymbol{c}_h) + Q^{n+1}(\mathbf{H}^* U^*, \boldsymbol{c}_h), \tag{3.36}$$

$$(\frac{a\phi_h^{n+1} - b\phi_h^n + c\phi_h^{n-1}}{2\delta t}, \varpi_h) + Q^{n+1}(\nabla \cdot (\phi^* \mathbf{u}^*), \varpi_h) = -M_2(\nabla \mu_h^{n+1}, \nabla \varpi_h), \tag{3.37}$$

$$(\mu_h^{n+1}, \psi_h) = \lambda(\nabla \phi_h^{n+1}, \nabla \psi_h) + S_{\phi}(\phi_h^{n+1}, \psi_h) + Q^{n+1}(R^* U^*, \psi_h), \tag{3.38}$$

$$(\frac{aU_h^{n+1} - bU_h^n + cU_h^{n-1}}{2\delta t}, V_h) = Q^{n+1}\left(\frac{1}{2}\mathbf{H}^* \cdot \mathbf{d}_t^* + \frac{1}{2} R^* \phi_t^*, V_h\right), \tag{3.39}$$

$$\begin{aligned}(\frac{a\tilde{\mathbf{u}}_h^{n+1} - b\mathbf{u}_h^n + c\mathbf{u}_h^{n-1}}{2\delta t}, \mathbf{v}_h) + Q^{n+1}((\mathbf{u}^* \cdot \nabla)\mathbf{u}^*, \mathbf{v}_h) + \nu(\nabla \tilde{\mathbf{u}}_h^{n+1}, \nabla \mathbf{v}_h) + (\nabla p_h^n, \mathbf{v}_h) \\ = Q^{n+1}\left(\boldsymbol{\omega}^* \nabla \mathbf{d}^* - \phi^* \nabla \mu^* - \frac{1-s}{2} \nabla \cdot (\mathbf{d}^* \boldsymbol{\omega}^*) + \frac{1+s}{2} \nabla \cdot (\boldsymbol{\omega}^* \mathbf{d}^*), \mathbf{v}_h\right),\end{aligned} \tag{3.40}$$

$$\begin{aligned}\frac{aQ^{n+1} - bQ^n + cQ^{n-1}}{2\delta t} = &((\mathbf{u}^* \cdot \nabla)\mathbf{u}^*, \tilde{\mathbf{u}}_h^{n+1}) + (\mathbf{u}^* \cdot \nabla \mathbf{d}^*, \boldsymbol{\omega}_h^{n+1}) - (\boldsymbol{\omega}^* \nabla \mathbf{d}^*, \tilde{\mathbf{u}}_h^{n+1}) \\ &+ (\nabla \cdot (\mathbf{u}^* \phi^*), \mu_h^{n+1}) + (\phi^* \nabla \mu^*, \tilde{\mathbf{u}}_h^{n+1}) \\ &+ \frac{1-s}{2}(\mathbf{d}^* \nabla \mathbf{u}^*, \boldsymbol{\omega}_h^{n+1}) + \frac{1-s}{2}(\nabla \cdot (\mathbf{d}^* \boldsymbol{\omega}^*), \tilde{\mathbf{u}}_h^{n+1}) \\ &- \frac{1+s}{2}(\mathbf{d}^* \cdot \nabla \mathbf{u}^*, \boldsymbol{\omega}_h^{n+1}) - \frac{1+s}{2}(\nabla \cdot (\boldsymbol{\omega}^* \mathbf{d}^*), \tilde{\mathbf{u}}_h^{n+1})\end{aligned} \tag{3.41}$$

$$-(\mathbf{H}^*\cdot\mathbf{d}_t^*,U_h^{n+1})+(\mathbf{H}^*U^*,\frac{a\mathbf{d}_h^{n+1}-b\mathbf{d}_h^n+c\mathbf{d}_h^{n-1}}{2\delta t})$$

$$-(R^*\phi_t^*,U_h^{n+1})+(R^*U^*,\frac{a\phi_h^{n+1}-b\phi_h^n+c\phi_h^{n-1}}{2\delta t}),$$

and

$$(\nabla(p_h^{n+1}-p_h^n),\nabla q_h)=-\frac{a}{2\delta t}(\nabla\cdot\tilde{\mathbf{u}}_h^{n+1},q_h), \tag{3.42}$$

$$\mathbf{u}_h^{n+1}=\tilde{\mathbf{u}}_h^{n+1}-\frac{2\delta t}{a}(\nabla p_h^{n+1}-\nabla p_h^n), \tag{3.43}$$

for all $\boldsymbol{m}_h\in Y_h^d$, $\mathbf{c}_h\in Y_h^d$, $\psi_h\in Y_h$, $w_h\in Y_h$, $\mathbf{v}_h\in\boldsymbol{V}_h$, $q_h\in O_h$, $V_h\in X_h$, where

$$\begin{cases}\mathbf{u}^*=2\mathbf{u}_h^n-\mathbf{u}_h^{n-1},\phi^*=2\phi_h^n-\phi_h^{n-1},\mu^*=2\mu_h^n-\mu_h^{n-1},\\ \mathbf{d}^*=2\phi_h^n-\phi_h^{n-1},\boldsymbol{\omega}^*=2\boldsymbol{\omega}_h^n-\boldsymbol{\omega}_h^{n-1},U^*=2U_h^n-U_h^{n-1},\\ \mathbf{H}^*=\mathbf{H}(\phi^*,\mathbf{d}^*),R^*=R(\phi^*,\mathbf{d}^*),\\ \phi_t^*=\dfrac{\tilde{a}\phi_h^n-\tilde{b}\phi_h^{n-1}+\tilde{c}\phi_h^{n-2}}{2\delta t},\mathbf{d}_t^*=\dfrac{\tilde{a}\mathbf{d}_h^n-\tilde{b}\mathbf{d}_h^{n-1}+\tilde{c}\mathbf{d}_h^{n-2}}{2\delta t},\\ a=3,b=4,c=1,\\ \tilde{a}=5,\tilde{b}=8,\tilde{c}=3.\end{cases} \tag{3.44}$$

Several remarks on the explanation of the developed scheme are given as follows.

Remark 3.5. In the above-developed numerical scheme (3.35)–(3.43), the initiation requires all variables at $t^1=\delta t$ and $t^2=2\delta t$, which can be achieved by using the first-order scheme. For instance, by using the backward Euler method for time derivative and first-order extrapolation method, we easily obtain a first-order scheme by setting $a=2,b=2,c=0,r^*=r^0,\forall r,\tilde{a}=2,\tilde{b}=2,\tilde{c}=0$ in (3.35)–(3.43). Meanwhile, the volume of ϕ^{n+1} is still valid, which can be shown by taking the L^2 inner product of (3.37) with 1 and applying the math induction (note that the first-order scheme also conserves the volume, thus ϕ_h^1 is also volume-conserved).

Remark 3.6. In the above-developed numerical scheme (3.35)–(3.43), the fluid equations are solved by using the second-order pressure-correction scheme. In this way, the calculation of pressure is independent of the velocity. This theoretical analysis of the second-order pressure-correction method is given in [33], where it is shown (discrete in time, continuous in space) that the velocity field follows the second-order accuracy, however, the pressure is only first-order accurate in time. The one-order loss of accuracy for the pressure is caused by the artificial Neumann boundary condition imposed on the pressure [34]. It is noted that the divergence-free condition in the discrete sense is automatically satisfied by the final velocity field $\mathbf{u}_h^n$, which can be deduced by taking the L^2 inner product of (3.43) with $\nabla q_h,q_h\in O_h$, that is

$$(\mathbf{u}_h^{n+1},\nabla q_h)=(-\nabla\cdot\tilde{\mathbf{u}}_h^{n+1},q_h)-\frac{2\delta t}{a}(\nabla(p_h^{n+1}-p_h^n),\nabla q_h). \tag{3.45}$$

Hence, from (3.42), we derive

$$(\mathbf{u}_h^{n+1},\nabla q_h)=0. \tag{3.46}$$

We now show that the scheme (3.35)–(3.43) is energy stable unconditionally. We will reuse the two identities as follows:

$$2(a-b,a)=|a|^2-|b|^2+|a-b|^2, \tag{3.47}$$

$$2(3a-4b+c)a=|a|^2-|b|^2+|2a-b|^2-|2b-c|^2+|a-2b+c|^2, \tag{3.48}$$

Theorem 3.1. *The scheme (3.35)–(3.43) follows an energy dissipation law, that reads as*

$$\frac{1}{\delta t}(E_h^{n+1}-E_h^n)\le-\nu\|\nabla\tilde{\mathbf{u}}_h^{n+1}\|^2-M_1\|\boldsymbol{\omega}_h^{n+1}\|^2-M_2\|\nabla\mu_h^{n+1}\|^2\le 0, \tag{3.49}$$

where

$$\begin{aligned} E_h^{n+1} =& \frac{1}{2}\Big(\frac{1}{2}\|\mathbf{u}_h^{n+1}\|^2+\frac{1}{2}\|2\mathbf{u}_h^{n+1}-\mathbf{u}_h^{n}\|^2\Big)+\frac{\delta t^2}{3}\|\nabla p_h^{n+1}\|^2 \\ &+\frac{\lambda}{2}\Big(\frac{1}{2}\|\nabla\phi_h^{n+1}\|^2+\frac{1}{2}\|2\nabla\phi_h^{n+1}-\nabla\phi_h^{n}\|^2\Big)+\frac{S_\phi}{2}\Big(\frac{1}{2}\|\phi_h^{n+1}\|^2+\frac{1}{2}\|2\phi_h^{n+1}-\phi_h^{n}\|^2\Big) \\ &+\frac{K}{2}\Big(\frac{1}{2}\|\nabla\mathbf{d}_h^{n+1}\|^2+\frac{1}{2}\|2\nabla\mathbf{d}_h^{n+1}-\nabla\mathbf{d}_h^{n}\|^2\Big)+\frac{S_\mathbf{d}}{2}\Big(\frac{1}{2}\|\mathbf{d}_h^{n+1}\|^2+\frac{1}{2}\|2\mathbf{d}_h^{n+1}-\mathbf{d}_h^{n}\|^2\Big) \\ &+\Big(\frac{1}{2}\|U_h^{n+1}\|^2+\frac{1}{2}\|2U_h^{n+1}-U_h^{n}\|^2\Big)+\frac{1}{2}\Big(\frac{1}{2}|Q^{n+1}|^2+\frac{1}{2}|2Q^{n+1}-Q^{n}|^2\Big)-B|\Omega|-\frac{1}{2}. \end{aligned} \tag{3.50}$$

Proof. By setting $\mathbf{v}_h = 2\delta t\tilde{\mathbf{u}}_h^{n+1}$ in (3.40), we get

$$\begin{aligned} &(3\tilde{\mathbf{u}}_h^{n+1}-4\mathbf{u}_h^{n}+\mathbf{u}_h^{n-1},\tilde{\mathbf{u}}_h^{n+1})+2\nu\delta t\|\nabla\tilde{\mathbf{u}}_h^{n+1}\|^2+2\delta t(\nabla p_h^{n},\tilde{\mathbf{u}}_h^{n+1}) \\ &\quad=-2\delta t\,Q^{n+1}((\mathbf{u}^*\cdot\nabla)\mathbf{u}^*,\tilde{\mathbf{u}}_h^{n+1})+2\delta t\,Q^{n+1}(\boldsymbol{\omega}^*\nabla\mathbf{d}^*,\tilde{\mathbf{u}}_h^{n+1})-2\delta t\,Q^{n+1}(\phi^*\nabla\mu^*,\tilde{\mathbf{u}}_h^{n+1}) \\ &\quad\quad-\frac{1-s}{2}2\delta t\,Q^{n+1}(\nabla\cdot(\mathbf{d}^*\boldsymbol{\omega}^*),\tilde{\mathbf{u}}_h^{n+1})+\frac{1+s}{2}2\delta t\,Q^{n+1}(\nabla\cdot(\boldsymbol{\omega}^*\mathbf{d}^*),\tilde{\mathbf{u}}_h^{n+1}). \end{aligned} \tag{3.51}$$

We rewrite (3.43) as

$$\tilde{\mathbf{u}}_h^{n+1}-\mathbf{u}_h^{n+1}=\frac{2\delta t}{3}\nabla(p_h^{n+1}-p_h^{n}). \tag{3.52}$$

Taking the L^2 inner product of the above equality with $\mathbf{u}_h^{n+1}$, we derive

$$(\tilde{\mathbf{u}}_h^{n+1}-\mathbf{u}_h^{n+1},\mathbf{u}_h^{n+1})=\frac{2\delta t}{3}(\nabla(p_h^{n+1}-p_h^{n}),\mathbf{u}_h^{n+1})=0, \tag{3.53}$$

and

$$\begin{aligned} &(3\mathbf{u}_h^{n+1}-4\mathbf{u}_h^{n}+\mathbf{u}_h^{n-1},\tilde{\mathbf{u}}_h^{n+1}-\mathbf{u}_h^{n+1}) \\ &\quad=(3\mathbf{u}_h^{n+1}-4\mathbf{u}_h^{n}+\mathbf{u}_h^{n-1},\frac{2\delta t}{3}\nabla(p_h^{n+1}-p_h^{n}))=0, \end{aligned} \tag{3.54}$$

where (3.46) is used.

By using (3.53) and (3.54), we deduce

$$\begin{aligned} &(3\tilde{\mathbf{u}}_h^{n+1}-4\mathbf{u}_h^{n}+\mathbf{u}_h^{n-1},\tilde{\mathbf{u}}_h^{n+1}) \\ &\quad=\big(3\tilde{\mathbf{u}}_h^{n+1}-3\mathbf{u}_h^{n+1},\tilde{\mathbf{u}}_h^{n+1}\big)+\big(3\mathbf{u}_h^{n+1}-4\mathbf{u}_h^{n}+\mathbf{u}_h^{n-1},\tilde{\mathbf{u}}_h^{n+1}\big) \\ &\quad=\big(3\tilde{\mathbf{u}}_h^{n+1}-3\mathbf{u}_h^{n+1},\tilde{\mathbf{u}}_h^{n+1}+\mathbf{u}_h^{n+1}\big)+\big(3\mathbf{u}_h^{n+1}-4\mathbf{u}_h^{n}+\mathbf{u}_h^{n-1},\mathbf{u}_h^{n+1}\big) \\ &\quad=\frac{1}{2}(\|\mathbf{u}_h^{n+1}\|^2-\|\mathbf{u}_h^{n}\|^2+\|2\mathbf{u}_h^{n+1}-\mathbf{u}_h^{n}\|^2-\|2\mathbf{u}_h^{n}-\mathbf{u}_h^{n-1}\|^2+\|\mathbf{u}_h^{n+1}-2\mathbf{u}_h^{n}+\mathbf{u}_h^{n-1}\|^2) \\ &\quad\quad+3\|\tilde{\mathbf{u}}_h^{n+1}\|^2-3\|\mathbf{u}_h^{n+1}\|^2. \end{aligned} \tag{3.55}$$

We rewrite (3.43) as

$$\mathbf{u}_h^{n+1}+\frac{2}{3}\delta t\nabla p_h^{n+1}=\tilde{\mathbf{u}}_h^{n+1}+\tfrac{2}{3}\delta t\nabla p_h^{n}.$$

Taking the inner product of the above equation with itself in L^2, and multiplying the obtained equation with $\frac{3}{2}$, we derive

$$2\delta t(\tilde{\mathbf{u}}_h^{n+1},\nabla p_h^{n})=\frac{3}{2}\|\mathbf{u}_h^{n+1}\|^2-\frac{3}{2}\|\tilde{\mathbf{u}}_h^{n+1}\|^2+\frac{2\delta t^2}{3}\|\nabla p_h^{n+1}\|^2-\frac{2\delta t^2}{3}\|\nabla p_h^{n}\|^2. \tag{3.56}$$

We rewrite (3.43) as

$$\mathbf{u}_h^{n+1}-\tilde{\mathbf{u}}_h^{n+1}=-\frac{2}{3}\delta t\nabla p_h^{n+1}+\frac{2}{3}\delta t\nabla p_h^{n}. \tag{3.57}$$

By taking the L^2 inner product of the above equation with $\frac{3}{2}\mathbf{u}_h^{n+1}$ and using (3.46), we obtain

$$\frac{3}{2}\|\mathbf{u}_h^{n+1}-\tilde{\mathbf{u}}_h^{n+1}\|^2+\frac{3}{2}\|\mathbf{u}_h^{n+1}\|^2=\frac{3}{2}\|\tilde{\mathbf{u}}_h^{n+1}\|^2. \tag{3.58}$$

By combining (3.51), (3.55), (3.56) and (3.58), we derive

$$\begin{aligned}
&\frac{1}{2}(\|\mathbf{u}_h^{n+1}\|^2-\|\mathbf{u}_h^{n}\|^2+\|2\mathbf{u}_h^{n+1}-\mathbf{u}_h^{n}\|^2-\|2\mathbf{u}_h^{n}-\mathbf{u}_h^{n-1}\|^2+\|\mathbf{u}_h^{n+1}-2\mathbf{u}_h^{n}+\mathbf{u}_h^{n-1}\|^2)\\
&\quad+\frac{3}{2}\|\mathbf{u}_h^{n+1}-\tilde{\mathbf{u}}_h^{n+1}\|^2+2\nu\delta t\|\nabla\tilde{\mathbf{u}}_h^{n+1}\|^2+\frac{2\delta t^2}{3}\|\nabla p_h^{n+1}\|^2-\frac{2\delta t^2}{3}\|\nabla p_h^{n}\|^2\\
&=\underbrace{-2\delta t\,Q^{n+1}((\mathbf{u}^*\cdot\nabla)\mathbf{u}^*,\tilde{\mathbf{u}}_h^{n+1})}_{\mathbb{M}_1}+\underbrace{2\delta t\,Q^{n+1}(\boldsymbol{\omega}^*\nabla\mathbf{d}^*,\tilde{\mathbf{u}}_h^{n+1})}_{\mathbb{C}_1}\underbrace{-2\delta t\,Q^{n+1}(\phi^*\nabla\mu^*,\tilde{\mathbf{u}}_h^{n+1})}_{\mathbb{D}_1}\\
&\quad\underbrace{-\frac{1-s}{2}2\delta t\,Q^{n+1}(\nabla\cdot(\mathbf{d}^*\boldsymbol{\omega}^*),\tilde{\mathbf{u}}_h^{n+1})}_{\mathbb{G}_1}+\underbrace{\frac{1+s}{2}2\delta t\,Q^{n+1}(\nabla\cdot(\boldsymbol{\omega}^*\mathbf{d}^*),\tilde{\mathbf{u}}_h^{n+1})}_{\mathbb{H}_1}.
\end{aligned}\tag{3.59}$$

By setting $\boldsymbol{m}_h=2\delta t\boldsymbol{\omega}_h^{n+1}$ in (3.35), we get

$$\begin{aligned}
(3\mathbf{d}_h^{n+1}-4\mathbf{d}_h^{n}+\mathbf{d}_h^{n-1},\boldsymbol{\omega}_h^{n+1})=-2\delta t M_1\|\boldsymbol{\omega}_h^{n+1}\|^2\underbrace{-2\delta t\,Q^{n+1}(\mathbf{u}^*\cdot\nabla\mathbf{d}^*,\boldsymbol{\omega}_h^{n+1})}_{\mathbb{A}_1}\\
\underbrace{-\frac{1-s}{2}2\delta t\,Q^{n+1}(\mathbf{d}^*\nabla\mathbf{u}^*,\boldsymbol{\omega}_h^{n+1})}_{\mathbb{E}_1}+\underbrace{\frac{1+s}{2}2\delta t\,Q^{n+1}(\mathbf{d}^*\cdot\nabla\mathbf{u}^*,\boldsymbol{\omega}_h^{n+1})}_{\mathbb{F}_1}.
\end{aligned}\tag{3.60}$$

By setting $\mathbf{c}_h=-(3\mathbf{d}_h^{n+1}-4\mathbf{d}_h^{n}+\mathbf{d}_h^{n-1})$ in (3.36), we get

$$\begin{aligned}
-(\boldsymbol{\omega}_h^{n+1},3\mathbf{d}_h^{n+1}-4\mathbf{d}_h^{n}+\mathbf{d}_h^{n-1})+K(\nabla\mathbf{d}_h^{n+1},\nabla(3\mathbf{d}_h^{n+1}-4\mathbf{d}_h^{n}+\mathbf{d}_h^{n-1}))\\
+S_{\mathbf{d}}(\mathbf{d}_h^{n+1},3\mathbf{d}_h^{n+1}-4\mathbf{d}_h^{n}+\mathbf{d}_h^{n-1})\\
=\underbrace{-Q^{n+1}(\mathbf{H}^*U^*,3\mathbf{d}_h^{n+1}-4\mathbf{d}_h^{n}+\mathbf{d}_h^{n-1})}_{\mathbb{I}_1}.
\end{aligned}\tag{3.61}$$

By setting $\varpi_h=2\delta t\mu_h^{n+1}$ in (3.37), we have

$$(3\phi_h^{n+1}-4\phi_h^{n}+\phi_h^{n-1},\mu_h^{n+1})=-2\delta t M_2\|\nabla\mu_h^{n+1}\|^2\underbrace{-2\delta t\,Q^{n+1}(\nabla\cdot(\mathbf{u}^*\phi^*),\mu_h^{n+1})}_{\mathbb{B}_1}.\tag{3.62}$$

By setting $\psi_h=-(3\phi_h^{n+1}-4\phi_h^{n}+\phi_h^{n-1})$ in (3.38), we find

$$\begin{aligned}
-(\mu_h^{n+1},3\phi_h^{n+1}-4\phi_h^{n}+\phi_h^{n-1})+\lambda(\nabla\phi_h^{n+1},\nabla(3\phi_h^{n+1}-4\phi_h^{n}+\phi_h^{n-1}))\\
+S_{\phi}(\phi_h^{n+1},3\phi_h^{n+1}-4\phi_h^{n}+\phi_h^{n-1})\\
=\underbrace{-Q^{n+1}(R^*U^*,3\phi_h^{n+1}-4\phi_h^{n}+\phi_h^{n-1})}_{\mathbb{J}_1}.
\end{aligned}\tag{3.63}$$

By setting $V_h=4\delta tU_h^{n+1}$ in (3.39), and using (3.48), we obtain

$$\begin{aligned}
\|U_h^{n+1}\|^2-\|U_h^{n}\|^2+\|2U_h^{n+1}-U_h^{n}\|^2-\|2U_h^{n}-U_h^{n-1}\|^2+\|U_h^{n+1}-2U_h^{n}+U_h^{n-1}\|^2\\
=\underbrace{2\delta t\,Q^{n+1}(\mathbf{H}^*\cdot\mathbf{d}_t^*,U_h^{n+1})}_{\mathbb{K}_1}+\underbrace{2\delta t\,Q^{n+1}(R^*\phi_t^*,U_h^{n+1})}_{\mathbb{L}_1}.
\end{aligned}\tag{3.64}$$

By multiplying (3.41) with $2\delta t\, Q^{n+1}$ and use (3.48) to obtain

$$\begin{aligned}
&\frac{1}{2}\Big(|Q^{n+1}|^2-|Q^n|^2+|2Q^{n+1}-Q^n|^2-|2Q^n-Q^{n-1}|^2+|Q^{n+1}-2Q^n+Q^{n-1}|^2\Big)\\
&=\underbrace{2\delta t\, Q^{n+1}(\mathbf{u}^*\cdot\nabla\mathbf{u}^*,\tilde{\mathbf{u}}_h^{n+1})}_{\mathbb{M}_2}+\underbrace{2\delta t\, Q^{n+1}(\mathbf{u}^*\cdot\nabla\mathbf{d}^*,\boldsymbol{\omega}_h^{n+1})}_{\mathbb{A}_2}\underbrace{-2\delta t\, Q^{n+1}(\boldsymbol{\omega}^*\nabla\mathbf{d}^*,\tilde{\mathbf{u}}_h^{n+1})}_{\mathbb{C}_2}\\
&\quad+\underbrace{2\delta t\, Q^{n+1}(\nabla\cdot(\mathbf{u}^*\phi^*),\mu_h^{n+1})}_{\mathbb{B}_2}+\underbrace{2\delta t\, Q^{n+1}(\phi^*\nabla\mu^*,\tilde{\mathbf{u}}_h^{n+1})}_{\mathbb{D}_2}\\
&\quad+\underbrace{\frac{1-s}{2}2\delta t\, Q^{n+1}(\mathbf{d}^*\nabla\mathbf{u}^*,\boldsymbol{\omega}_h^{n+1})}_{\mathbb{E}_2}+\underbrace{\frac{1-s}{2}2\delta t\, Q^{n+1}(\nabla\cdot(\mathbf{d}^*\boldsymbol{\omega}^*),\tilde{\mathbf{u}}_h^{n+1})}_{\mathbb{G}_2}\\
&\quad\underbrace{-\frac{1+s}{2}2\delta t\, Q^{n+1}(\mathbf{d}^*\cdot\nabla\mathbf{u}^*,\boldsymbol{\omega}_h^{n+1})}_{\mathbb{F}_2}\underbrace{-\frac{1+s}{2}2\delta t\, Q^{n+1}(\nabla\cdot(\boldsymbol{\omega}^*\mathbf{d}^*),\tilde{\mathbf{u}}_h^{n+1})}_{\mathbb{H}_2}\\
&\quad\underbrace{-2\delta t\, Q^{n+1}(\mathbf{H}^*\cdot\mathbf{d}_t^*,U_h^{n+1})}_{\mathbb{K}_2}+\underbrace{Q^{n+1}(\mathbf{H}^*U^*,3\mathbf{d}_h^{n+1}-4\mathbf{d}_h^n+\mathbf{d}_h^{n-1})}_{\mathbb{I}_2}\\
&\quad\underbrace{-2\delta t\, Q^{n+1}(R^*\phi_t^*,U_h^{n+1})}_{\mathbb{L}_2}+\underbrace{Q^{n+1}(R^*U^*,3\phi_h^{n+1}-4\phi_h^n+\phi_h^{n-1})}_{\mathbb{J}_2},
\end{aligned}\tag{3.65}$$

Hence, by combining (3.59)–(3.65) and using (3.47)–(3.48), we arrive at

$$\begin{aligned}
&\frac{1}{2}(\|\mathbf{u}_h^{n+1}\|^2-\|\mathbf{u}_h^n\|^2+\|2\mathbf{u}_h^{n+1}-\mathbf{u}_h^n\|^2-\|2\mathbf{u}_h^n-\mathbf{u}_h^{n-1}\|^2)+\frac{2}{3}\delta t^2(\|\nabla p_h^{n+1}\|^2-\|\nabla p_h^n\|^2)\\
&\quad+\frac{K}{2}(\|\nabla\mathbf{d}_h^{n+1}\|^2-\|\nabla\mathbf{d}_h^n\|^2+\|\nabla(2\mathbf{d}_h^{n+1}-\mathbf{d}_h^n)\|^2-\|\nabla(2\mathbf{d}_h^n-\mathbf{d}_h^{n-1})\|^2)\\
&\quad+\frac{S_{\mathbf{d}}}{2}(\|\mathbf{d}_h^{n+1}\|^2-\|\mathbf{d}_h^n\|^2+\|2\mathbf{d}_h^{n+1}-\mathbf{d}_h^n\|^2-\|2\mathbf{d}_h^n-\mathbf{d}_h^{n-1}\|^2)\\
&\quad+\frac{\lambda}{2}(\|\nabla\phi_h^{n+1}\|^2-\|\nabla\phi_h^n\|^2+\|\nabla(2\phi_h^{n+1}-\phi_h^n)\|^2-\|\nabla(2\phi_h^n-\phi_h^{n-1})\|^2)\\
&\quad+\frac{S_\phi}{2}(\|\phi_h^{n+1}\|^2-\|\phi_h^n\|^2+\|2\phi_h^{n+1}-\phi_h^n\|^2-\|2\phi_h^n-\phi_h^{n-1}\|^2)\\
&\quad+(\|U_h^{n+1}\|^2-\|U_h^n\|^2+\|2U_h^{n+1}-U_h^n\|^2-\|2U_h^n-U_h^{n-1}\|^2)\\
&\quad+\frac{1}{2}(|Q^{n+1}|^2-|Q^n|^2+|2Q^{n+1}-Q^n|^2-|2Q^n-Q^{n-1}|^2)\\
&\quad+\Big\{\frac{1}{2}\|\mathbf{u}_h^{n+1}-2\mathbf{u}_h^n+\mathbf{u}_h^{n-1}\|^2+\frac{3}{2}\|\mathbf{u}_h^{n+1}-\tilde{\mathbf{u}}_h^{n+1}\|^2\\
&\qquad+\frac{\lambda}{2}\|\nabla(\phi_h^{n+1}-2\phi_h^n+\phi_h^{n-1})\|^2+\frac{S_\phi}{2}\|\phi_h^{n+1}-2\phi_h^n+\phi_h^{n-1}\|^2\\
&\qquad+\frac{K}{2}\|\nabla(\mathbf{d}_h^{n+1}-2\mathbf{d}_h^n+\mathbf{d}_h^{n-1})\|^2+\frac{S_{\mathbf{d}}}{2}\|\mathbf{d}_h^{n+1}-2\mathbf{d}_h^n+\mathbf{d}_h^{n-1}\|^2\\
&\qquad+\|U_h^{n+1}-2U_h^n+U_h^{n-1}\|^2+\frac{1}{2}|Q^{n+1}-2Q^n+Q^{n-1}|^2\Big\}\\
&=-2\delta t\nu\|\nabla\tilde{\mathbf{u}}_h^{n+1}\|^2-2\delta t M_1\|\boldsymbol{\omega}_h^{n+1}\|^2-2\delta t M_2\|\nabla\mu_h^{n+1}\|^2,
\end{aligned}\tag{3.66}$$

where all terms marked with same letters are canceled.

Finally, the energy law (3.49) is obtained after we drop the positive terms in { } from (3.66). □

3.3. Decoupled implementation

In this subsection, we introduce the decoupling implementation process for the scheme (3.35)–(3.43). The key idea is to apply the nonlocal feature of the auxiliary variable Q, which will be fully utilized to split other local

variables into a form of linear combination. In other words, since Q is a nonlocal scalar, any variable ψ can always be split into the form of

$$\psi = \psi_1 + Q^{n+1}\psi_2. \tag{3.67}$$

Using the nonlocal attribute of the auxiliary variable Q, we split all variables into multiple variables and then merge them back.

Step 1:, we split $\mathbf{d}_h^{n+1}, \boldsymbol{\omega}_h^{n+1}, \phi_h^{n+1}, \mu_h^{n+1}$ into a linear combination form in terms of Q^{n+1}, namely,

$$\begin{cases} \mathbf{d}_h^{n+1} = \mathbf{d}_{h1}^{n+1} + Q^{n+1}\mathbf{d}_{h2}^{n+1}, \boldsymbol{\omega}_h^{n+1} = \boldsymbol{\omega}_{h1}^{n+1} + Q^{n+1}\boldsymbol{\omega}_{h2}^{n+1}, \\ \phi_h^{n+1} = \phi_{h1}^{n+1} + Q^{n+1}\phi_{h2}^{n+1}, \mu_h^{n+1} = \mu_{h1}^{n+1} + Q^{n+1}\mu_{h2}^{n+1}. \end{cases} \tag{3.68}$$

We solve $\mathbf{d}_{hi}^{n+1}, \boldsymbol{\omega}_{hi}^{n+1}, \phi_{hi}^{n+1}, \mu_{hi}^{n+1}$ for $i = 1, 2$, as follows.

Using (3.68), we replace $\mathbf{d}_h^{n+1}, \boldsymbol{\omega}_h^{n+1}, \phi_h^{n+1}, \mu_h^{n+1}$ in the system (3.35)–(3.38), and decompose the obtained equations according to Q^{n+1} into the following four subsystems:

$$\begin{cases} \dfrac{a}{2M_1\delta t}(\mathbf{d}_{h1}^{n+1}, \boldsymbol{m}_h) = -(\boldsymbol{\omega}_{h1}^{n+1}, \boldsymbol{m}_h) + G_1, \\ (\boldsymbol{\omega}_{h1}^{n+1}, \mathbf{c}_h) = K(\nabla\mathbf{d}_{h1}^{n+1}, \nabla\mathbf{c}_h) + S_{\mathbf{d}}(\mathbf{d}_{h1}^{n+1}, \mathbf{c}_h), \end{cases} \tag{3.69}$$

$$\begin{cases} \dfrac{a}{2M_1\delta t}(\mathbf{d}_{h2}^{n+1}, \boldsymbol{m}_h) = -(\boldsymbol{\omega}_{h2}^{n+1}, \boldsymbol{m}_h) + G_2, \\ (\boldsymbol{\omega}_{h2}^{n+1}, \mathbf{c}_h) = K(\nabla\mathbf{d}_{h2}^{n+1}, \nabla\mathbf{c}_h) + S_{\mathbf{d}}(\mathbf{d}_{h2}^{n+1}, \mathbf{c}_h) + G_3, \end{cases} \tag{3.70}$$

$$\begin{cases} \dfrac{a}{2M_2\delta t}(\phi_{h1}^{n+1}, \varpi_h) = -(\nabla\mu_{h1}^{n+1}, \nabla\varpi_h) + G_4, \\ (\mu_{h1}^{n+1}, \psi_h) = \lambda(\nabla\phi_{h1}^{n+1}, \nabla\psi_h) + S_\phi(\phi_{h1}^{n+1}, \psi_h), \end{cases} \tag{3.71}$$

$$\begin{cases} \dfrac{a}{2M_2\delta t}(\phi_{h2}^{n+1}, \varpi_h) = -(\nabla\mu_{h2}^{n+1}, \nabla\varpi_h) + G_5, \\ (\mu_{h2}^{n+1}, \psi_h) = \lambda(\nabla\phi_{h2}^{n+1}, \nabla\psi_h) + S_\phi(\phi_{h2}^{n+1}, \psi_h) + G_6. \end{cases} \tag{3.72}$$

where

$$\begin{cases} G_1 = \dfrac{1}{M_1}\Big(\dfrac{b\mathbf{d}_h^n - c\mathbf{d}_h^{n-1}}{2\delta t}, \boldsymbol{m}_h\Big), \\ G_2 = \dfrac{1}{M_1}\Big(-\mathbf{u}^*\cdot\nabla\mathbf{d}^* - \dfrac{1-s}{2}\mathbf{d}^*\nabla\mathbf{u}^* + \dfrac{1+s}{2}\mathbf{d}^*\cdot\nabla\mathbf{u}^*, \boldsymbol{m}_h\Big), G_3 = (\mathbf{H}^*U^*, \mathbf{c}_h), \\ G_4 = \dfrac{1}{M_2}\Big(\dfrac{b\phi^n - c\phi^{n-1}}{2\delta t}, \varpi_h\Big), G_5 = \dfrac{1}{M_2}\Big(-\nabla\cdot(\phi^*\mathbf{u}^*), \varpi_h\Big), G_6 = (R^*U^*, \psi_h). \end{cases} \tag{3.73}$$

It is easy to solve (3.69)–(3.72) since these four systems are linear and decoupled, G_i $(i = 1, \ldots, 6)$ are all known terms. Meanwhile, all equations in these systems are elliptic and constant-coefficient.

Step 2. We further use Q^{n+1} to split U_h^{n+1} as

$$U_h^{n+1} = U_{1h}^{n+1} + Q^{n+1}U_{2h}^{n+1}. \tag{3.74}$$

Using (3.74), Eq. (3.39) is rewritten as the following form:

$$\frac{a}{2\delta t}(U_{1h}^{n+1}, V_h) = (\frac{bU_h^n - cU_h^{n-1}}{2\delta t}, V_h), \tag{3.75}$$

$$\frac{a}{2\delta t}(U_{2h}^{n+1}, V_h) = (\frac{1}{2}\mathbf{H}^*\phi_t^* + \frac{1}{2}R^*\phi_t^*, V_h). \tag{3.76}$$

These two equations are easy to solve because all the terms on the right are known.

Step 3. Using Q^{n+1}, we split the velocity field $\tilde{\mathbf{u}}_h^{n+1}$ as

$$\tilde{\mathbf{u}}_h^{n+1} = \tilde{\mathbf{u}}_{1h}^{n+1} + Q^{n+1}\tilde{\mathbf{u}}_{2h}^{n+1}. \tag{3.77}$$

After replacing the variable $\tilde{\mathbf{u}}_h^{n+1}$ in (3.40), and splitting the obtained equations in terms of Q^{n+1}, we can obtain two sub-systems:

$$\frac{a}{2\delta t}(\tilde{\mathbf{u}}_{1h}^{n+1}, \mathbf{v}_h) + \nu(\nabla\tilde{\mathbf{u}}_{1h}^{n+1}, \nabla\mathbf{v}_h) = (-\nabla p_h^n + \frac{b\mathbf{u}_h^n - c\mathbf{u}_h^{n-1}}{2\delta t}, \mathbf{v}_h), \tag{3.78}$$

$$\frac{a}{2\delta t}(\tilde{\mathbf{u}}_{2h}^{n+1}, \mathbf{v}_h) + \nu(\nabla\tilde{\mathbf{u}}_{2h}^{n+1}, \nabla\mathbf{v}_h) = (-(\mathbf{u}^*\cdot\nabla)\mathbf{u}^*, \mathbf{v}_h) \tag{3.79}$$
$$-\left(\boldsymbol{\omega}^*\nabla\mathbf{d}^* - \phi^*\nabla\mu^* - \frac{1-s}{2}\nabla\cdot(\mathbf{d}^*\boldsymbol{\omega}^*) + \frac{1+s}{2}\nabla\cdot(\boldsymbol{\omega}^*\mathbf{d}^*), \mathbf{v}_h\right).$$

It is easy to solve (3.78)–(3.79) since they are constant-coefficient elliptic equations.

Step 4: we solve Q^{n+1} in (3.41). By using the linear combination forms for the variables $\boldsymbol{\omega}_h^{n+1}$, μ_h^{n+1} in (3.68), $\tilde{\mathbf{u}}^{n+1}$ in (3.77), we formulate (3.41) into the following form:

$$(\frac{3}{2\delta t} - \eta_2)Q^{n+1} = \frac{1}{2\delta t}(4Q^n - Q^{n-1}) + \eta_1, \tag{3.80}$$

where $\eta_i, i = 1, 2$ are given as

$$\begin{aligned}
\eta_1 = {} & ((\mathbf{u}^*\cdot\nabla)\mathbf{u}^*, \tilde{\mathbf{u}}_{h1}^{n+1}) + (\mathbf{u}^*\cdot\nabla\mathbf{d}^*, \boldsymbol{\omega}_{h1}^{n+1}) - (\boldsymbol{\omega}^*\nabla\mathbf{d}^*, \tilde{\mathbf{u}}_{h1}^{n+1}) \\
& + (\nabla\cdot(\phi^*\mathbf{u}^*), \mu_{h1}^{n+1}) + (\phi^*\nabla\mu^*, \tilde{\mathbf{u}}_{h1}^{n+1}) \\
& + \frac{1-s}{2}(\mathbf{d}^*\nabla\mathbf{u}^*, \boldsymbol{\omega}_{h1}^{n+1}) + \frac{1-s}{2}(\nabla\cdot(\mathbf{d}^*\boldsymbol{\omega}^*), \tilde{\mathbf{u}}_{h1}^{n+1}) \\
& - \frac{1+s}{2}(\mathbf{d}^*\cdot\nabla\mathbf{u}^*, \boldsymbol{\omega}_{h1}^{n+1}) - \frac{1+s}{2}(\nabla\cdot(\boldsymbol{\omega}^*\mathbf{d}^*), \tilde{\mathbf{u}}_{h1}^{n+1}) \\
& - (\mathbf{H}^*\cdot\mathbf{d}_t^*, U_{h1}^{n+1}) + (\mathbf{H}^*U^*, \frac{a\mathbf{d}_{h1}^{n+1} - b\mathbf{d}_h^n + c\mathbf{d}_h^{n-1}}{2\delta t}) \\
& - (R^*\phi_t^*, U_{h1}^{n+1}) + (R^*U^*, \frac{a\phi_{h1}^{n+1} - b\phi_h^n + c\phi_h^{n-1}}{2\delta t}),
\end{aligned}$$

$$\begin{aligned}
\eta_2 = {} & ((\mathbf{u}^*\cdot\nabla)\mathbf{u}^*, \tilde{\mathbf{u}}_{h2}^{n+1}) + (\mathbf{u}^*\cdot\nabla\mathbf{d}^*, \boldsymbol{\omega}_{h2}^{n+1}) - (\boldsymbol{\omega}^*\nabla\mathbf{d}^*, \tilde{\mathbf{u}}_{h2}^{n+1}) \\
& + (\nabla\cdot(\phi^*\mathbf{u}^*), \mu_{h2}^{n+1}) + (\phi^*\nabla\mu^*, \tilde{\mathbf{u}}_{h2}^{n+1}) \\
& + \frac{1-s}{2}(\mathbf{d}^*\nabla\mathbf{u}^*, \boldsymbol{\omega}_{h2}^{n+1}) + \frac{1-s}{2}(\nabla\cdot(\mathbf{d}^*\boldsymbol{\omega}^*), \tilde{\mathbf{u}}_{h2}^{n+1}) \\
& - \frac{1+s}{2}(\mathbf{d}^*\cdot\nabla\mathbf{u}^*, \boldsymbol{\omega}_{h2}^{n+1}) - \frac{1+s}{2}(\nabla\cdot(\boldsymbol{\omega}^*\mathbf{d}^*), \tilde{\mathbf{u}}_{h2}^{n+1}) \\
& - (\mathbf{H}^*\cdot\mathbf{d}_t^*, U_{h2}^{n+1}) - (R^*\phi_t^*, U_{h2}^{n+1}) + \frac{a}{2\delta t}(\mathbf{H}^*U^*, \mathbf{d}_{h2}^{n+1}) + \frac{a}{2\delta t}(R^*U^*, \phi_{h2}^{n+1}),
\end{aligned}$$

Because all terms contained in η_1 and η_2 have been already obtained from Step 1-Step 3 (solvability of (3.80) is given below), the linear algebraic equation (3.80) can be easily solved. Once Q^{n+1} is obtained from (3.80), we update $\tilde{\mathbf{u}}_h^{n+1}$ from (3.77), $\mathbf{d}_h^{n+1}$, $\boldsymbol{\omega}_h^{n+1}$, ϕ_h^{n+1}, μ_h^{n+1} from (3.68), and U_h^{n+1} from (3.74).

We further show the solvability of (3.80) by proving $\frac{3}{2\delta t} - \eta_2 \neq 0$. By setting $\mathbf{v}_h = \tilde{\mathbf{u}}_{h2}^{n+1}$ in (3.79), we deduce

$$\begin{aligned}
-((\mathbf{u}^*\cdot\nabla)\mathbf{u}^*, \tilde{\mathbf{u}}_{h2}^{n+1}) - (\phi^*\nabla\mu^*, \tilde{\mathbf{u}}_{h2}^{n+1}) + (\boldsymbol{\omega}^*\nabla\mathbf{d}^*, \tilde{\mathbf{u}}_{h2}^{n+1}) \\
- \frac{1-s}{2}(\nabla\cdot(\mathbf{d}^*\boldsymbol{\omega}^*), \tilde{\mathbf{u}}_{h2}^{n+1}) + \frac{1+s}{2}(\nabla\cdot(\boldsymbol{\omega}^*\mathbf{d}^*), \tilde{\mathbf{u}}_{h2}^{n+1}) \\
= \frac{a}{2\delta t}\|\tilde{\mathbf{u}}_{h2}^{n+1}\|^2 + \nu\|\nabla\tilde{\mathbf{u}}_{h2}^{n+1}\|^2 \geq 0.
\end{aligned} \tag{3.81}$$

By setting $\boldsymbol{m}_h = M_1\boldsymbol{\omega}_{h2}^{n+1}$, $\mathbf{c}_h = -\frac{a}{2\delta t}\mathbf{d}_{h2}^{n+1}$ in (3.70), $\varpi_h = M_2\mu_{h2}^{n+1}$, $\psi_h = -\frac{a}{2\delta t}\phi_{h2}^{n+1}$ in (3.72), and combining the four obtained equations, we get

$$\begin{aligned}
&-(\mathbf{u}^*\cdot\nabla\mathbf{d}^*,\boldsymbol{\omega}_{h2}^{n+1})-(\nabla\cdot(\phi^*\mathbf{u}^*),\mu_{h2}^{n+1})-\frac{1-s}{2}(\mathbf{d}^*\nabla\mathbf{u}^*,\boldsymbol{\omega}_{h2}^{n+1})+\frac{1+s}{2}(\mathbf{d}^*\cdot\nabla\mathbf{u}^*,\boldsymbol{\omega}_{h2}^{n+1})\\
&\quad-\frac{a}{2\delta t}\left((\mathbf{H}^*U^*,\mathbf{d}_{h2}^{n+1})-(R^*U^*,\phi_{h2}^{n+1})\right)\\
&=M_1\|\boldsymbol{\omega}_{h2}^{n+1}\|^2+\frac{aK}{2\delta t}\|\nabla\mathbf{d}_{h2}^{n+1}\|^2+\frac{aS_{\mathbf{d}}}{2\delta t}\|\mathbf{d}_{h2}^{n+1}\|^2+M_2\|\nabla\mu_{h2}^{n+1}\|^2\\
&\quad+\frac{a\lambda}{2\delta t}\|\nabla\phi_{h2}^{n+1}\|^2+\frac{aS_\phi}{2\delta t}\|\phi_{h2}^{n+1}\|^2\geq 0.
\end{aligned}\tag{3.82}$$

By setting $V_h = U_{h2}^{n+1}$ in (3.76), we get

$$(\mathbf{H}^*\cdot\mathbf{d}_t^*,U_{h2}^{n+1})+(R^*\phi_t^*,\phi_{h2}^{n+1})=\frac{a}{\delta t}\|U_{h2}^{n+1}\|^2\geq 0.\tag{3.83}$$

From (3.81), (3.82) and (3.83), we get $-\eta_2\geq 0$. Thus (3.80) is always solvable.

Step 5: we update p_h^{n+1} and $\mathbf{u}_h^{n+1}$ from (3.42) and (3.43).

Now we summarize the solution process described above. It can be seen that the calculation of all unknown variables has been completely decoupled, and all nonlinear terms will not bring any variable coefficients. In each time step, the total computational cost of the scheme is to solve several independent, constant-coefficient elliptic equations. The decoupling characteristics of the scheme and the fact that all equations are constant coefficients mean very effective actual calculations. In addition, although we consider only the proof of energy stability in this study, optimal error estimates are expected to be obtained without any essential difficulties. We will implement the subsequent error analysis in the future work by following the same lines as the available analytical work for hydrodynamically coupled Cahn–Hilliard model [28,35–39] and Navier–Stokes equations [33].

4. Numerical examples

In this section, we first implement several numerical examples to verify the convergence rate and energy stability of the proposed fully discrete scheme (3.35)–(3.43). Then, we implement several benchmark simulations on the special "beads-on-string" phenomenon of viscoelastic fluids to demonstrate the effectiveness of this scheme. In all the examples below, the Taylor–Hood elements [32] for $\boldsymbol{V}_h$ and O_h satisfying the inf–sup condition and the finite element spaces (3.25) with $l_1 = 1, l_2 = 2, l_3 = 1$ are used.

4.1. Tests of accuracy and stability

We perform refinement tests on the time step size δt and spatial grid size h to verify the convergence order of the proposed scheme (3.35)–(3.43). We set the 2D computational domain to $\Omega = [0, 2\pi]^2$. The initial conditions read as

$$\begin{cases}\phi^0=\dfrac{1}{2}\tanh\left(\dfrac{r_0-|\boldsymbol{x}-\boldsymbol{x}_0|}{2\epsilon}\right)+\dfrac{1}{2},\\ \mathbf{d}^0=(\mathbf{d}_1^0,\mathbf{d}_2^0)=(0,\phi^0),\ \mathbf{u}^0=(0,0),\ p^0=0,\end{cases}\tag{4.1}$$

with $r_0 = 1.3, \boldsymbol{x}_0 = (x_0, y_0) = (\pi, \pi)$.

We set the model parameters as follows,

$$\begin{cases}M_1=0.01,\epsilon=6\times10^{-2},\lambda=0.01,B=1,s=1.2,\phi_c=1/2,\\ M_2=1,K=0.01,\alpha=1,\nu_1=\nu_2=1,\gamma=1,\eta=0.01,\\ \tau=1,\beta=500,S_\phi=\dfrac{4}{\epsilon^2},S_{\mathbf{d}}=2,\end{cases}\tag{4.2}$$

where the three stabilization parameters $S_\phi\sim O(1/\epsilon^2)$, $S_{\mathbf{d}}\sim O(\alpha)$ (from Remark 3.3).

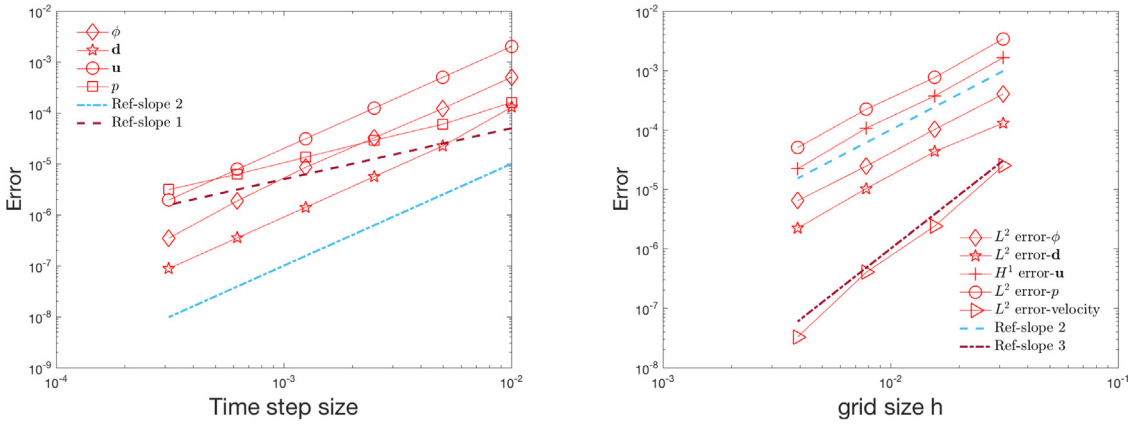

(a) Accuracy test in temporal discretization. (b) Accuracy test in spatial discretization.

Fig. 4.1. (a) The numerical errors in the L^2 space of all variables computed using various time steps δt, and (b) the numerical errors in the L^2 space of all variables computed using various spatial grid sizes h.

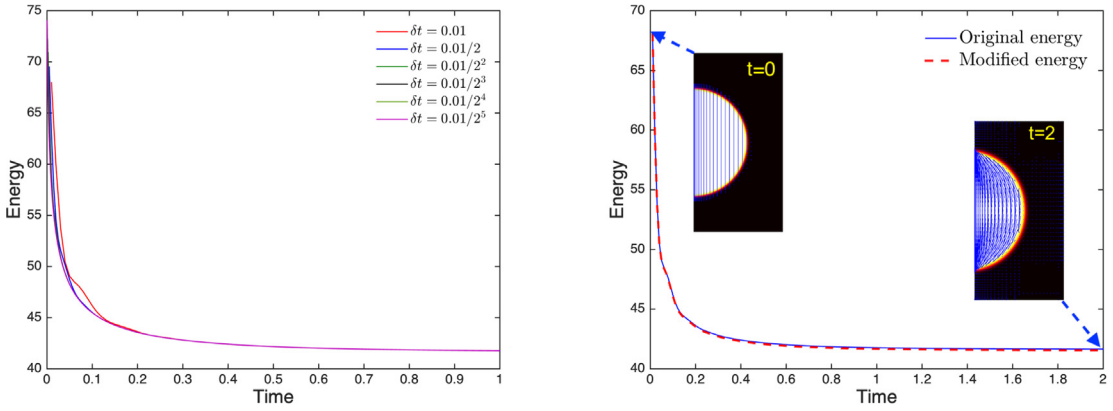

(a) Energy evolutions with various δt. (b) Original and modified energy with $\delta t = 0.01/2$.

Fig. 4.2. (a) Temporal evolution curves of the total free energy, which is obtained by six different time steps with a factor of $1/2$ for each; and (b) the comparisons of the original energy (2.15) and the modified energy (3.50) computed by using the time step $\delta t = 0.01/2$.

To verify the order of accuracy for discretization in time, we fix mesh size $h = 1/256$ so that the spatial grid size h is sufficiently small and the spatial discretization errors can be omitted if compared with the discretization error in time. In Fig. 4.1(a), the numerical errors between the numerical solution and the exact solution at $t = 1$ and in the L^2-space are plotted, where numerical solution computed by using very small time step ($\delta t = 1 \times 10^{-6}$) is treated as the exact solution. The scheme shows the second-order temporal accuracy of $\mathbf{u}, \phi, \mathbf{d}$ and the first-order temporal accuracy of p.

To verify the order of convergence of discretization in space, we show the numerical errors in Fig. 4.1(b) calculated using various grid sizes h. We choose δt sufficiently small ($\delta t = 1 \times 10^{-5}$) so that the errors are dominated by the spatial discretization error. We can see that the H^1-errors of the velocity follows the second-order convergence rate, which are also followed by the L^2-errors of the pressure p and the phase-field variable ϕ. The L^2-errors of the velocity field follow the third-order convergence rates. These results are completely consistent with the theoretical expectations of the accuracy of P_2/P_1 element for $(\mathbf{u}, p)$ and the P_1 element for $(\phi, \mathbf{d})$.

We continue to show whether the scheme is unconditionally energy stable by plotting energy evolution curves over time, shown in Fig. 4.2 (a), where we plot the temporal evolution curves of the total free energy (3.50), which is obtained by six different time steps with a factor $1/2$ for each. It can be seen that all the obtained energy curves show a monotonic decay trend, which shows that the scheme is energy-stable. In Fig. 4.2 (b), we plot the temporal

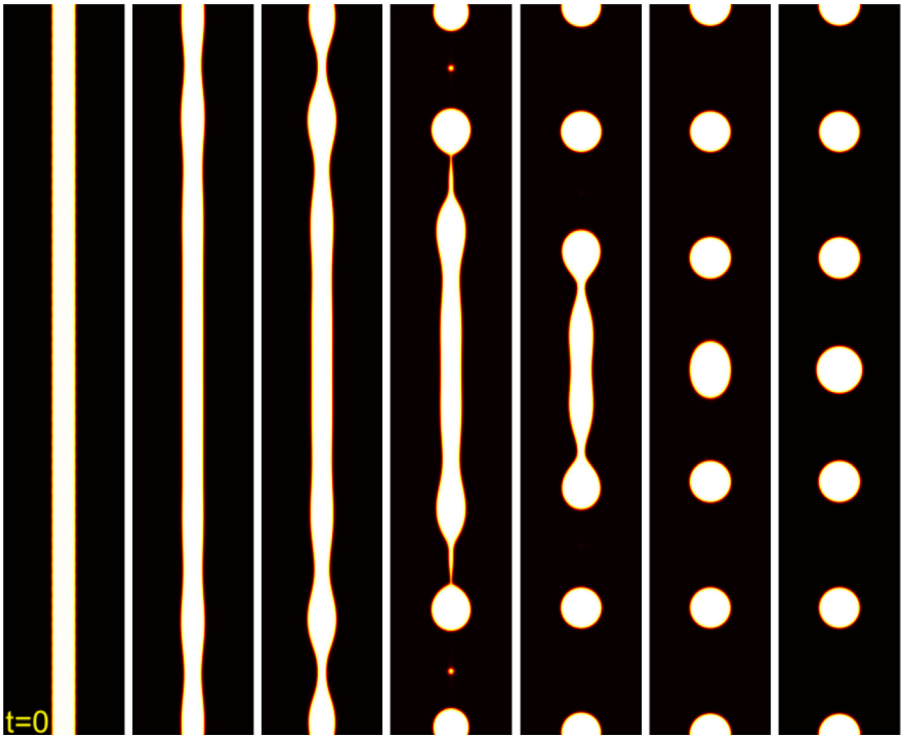

Fig. 4.3. The deformation of an axisymmetric viscous filament that is immersed in another viscous fluid, where the elastic constant is $K = 1 \times 10^{-5}$ and the anchoring constant is $\eta = 0$. The snapshots are taken at $t = 0, 6, 7, 8, 9, 10, 10.4$.

evolution curve of the total free energy (2.15) (in the original form) and (3.50) (in the modified discrete form) using $\delta t = 0.01/2$. We can see that the two energy curves are very consistent. We also attach the half-section of the phase-field variable ϕ and director-field $\mathbf{d}$ at $t = 0$ (initial) and $t = 2$ (steady state), where we can see that due to the parallel anchoring condition, the LC droplet slightly deforms, and the anchoring energy distorts the director field to align it with the droplet interface.

4.2. LC filament pinch-off: "beads-on-string" phenomenon

In this section, we simulate the "beads-on-string" phenomenon by setting the initial contour ϕ^0 to be a cylindrical filament. The computed domain $(r, z) \in \Omega$ is set to a cylinder with a radius of R and a height of L. For simplicity, we assume that the problem is axisymmetric, and the cylinder contains an immiscible mixture of viscous fluid and a cylindrical LC filament (placed along the axis of the cylinder) with the same viscosity and density.

The initial conditions read as

$$\begin{cases} \phi^0(r, z) = -\dfrac{1}{2}\tanh\left(2R_0^2/\epsilon\big(\dfrac{r^2}{R_0 + 0.001\text{rand}(r, z)}\big) - 1\right) + \dfrac{1}{2}, \\ \mathbf{d}^0 = (\mathbf{d}_1^0, \mathbf{d}_2^0) = (0, \phi^0), \mathbf{u}^0 = (0, 0), p^0 = 0, \end{cases} \tag{4.3}$$

where $R_0 = \frac{2}{11}R$ and rand(r, z) is the random number in $[-1, 1]$ which means that a very slight disturbance is applied to the filament radius. The initial profile of ϕ^0 is shown in the first subfigure of Fig. 4.3.

The model parameters are set as follows,

$$\begin{cases} R = 1, L = 12, M_1 = 1 \times 10^{-3}, \epsilon = 1.5 \times 10^{-2}, \lambda = 0.1, B = 1, \phi_c = 1/2, s = 1.2, \\ M_2 = 2 \times 10^{-3}, \alpha = 5, \nu = 1, \gamma = 1, S_\phi = 4/\epsilon^2, S_{\mathbf{d}} = 2, h = \dfrac{1}{256}, \delta t = 1 \times 10^{-4}. \end{cases} \tag{4.4}$$

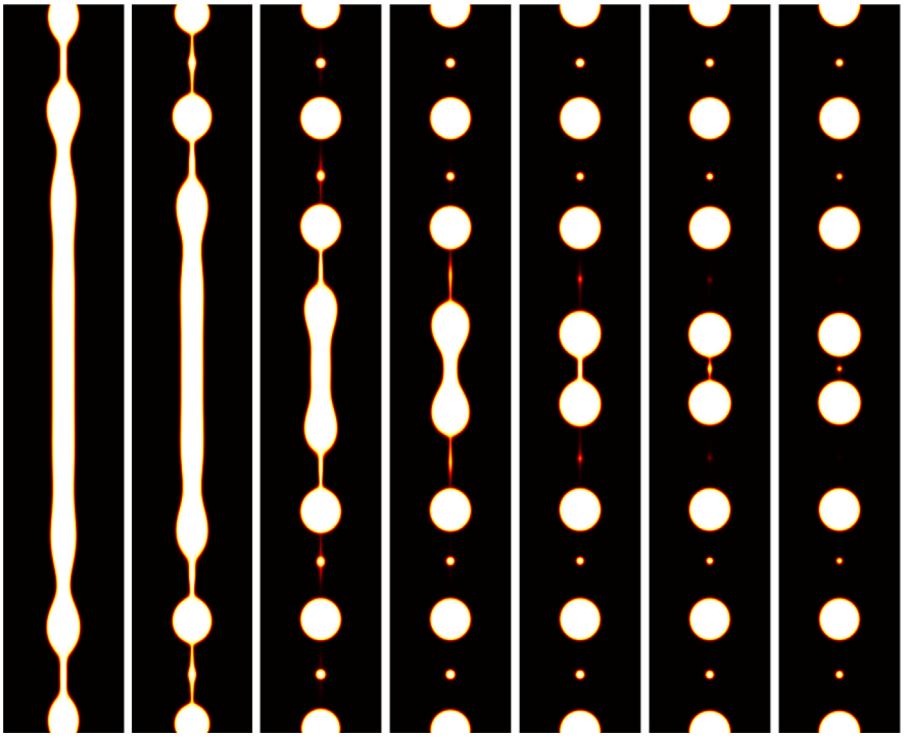

Fig. 4.4. The deformation of an axisymmetric LC filament that is immersed in another viscous fluid, where the elastic constant is $K = 1.2$ and the anchoring constant is $\eta = 12$. The snapshots are taken at $t = 1.8, 2, 2.4, 2.6, 2.8, 3, 3.2$.

To show the effect of elastic energy on the deformation dynamics of the LC filament, we first set the two parameters K and η very small, so that the elastic effect is very small, and the filament is very close to the viscous fluid. Then we increase the elastic constant K and the magnitude of the anchoring energy constant η to investigate the difference in the pinch-off phenomena of the LC fluid.

First, we set $K = 1 \times 10^{-5}$, $\eta = 0$ to make the filament approximate to a viscous fluid. The snapshots of ϕ at various times are shown in Fig. 4.3. We can see that the whole filament begins to become thinner in the upper and lower parts, and then breaks to form several small satellite droplets. Finally, the entire filament forms seven satellite droplets of a uniform size. This phenomenon is known as the Rayleigh instability, see [41]. It should be emphasized that the phenomenon of "beads-on-string" does not appear for the viscous filament.

Second, we set $K = 1.2$ and $\eta = 12$ to turn the filament into a LC fluid. The profiles of ϕ at various times are shown in Fig. 4.4. An obvious difference can be seen compared with the viscous filament in Fig. 4.3. For example, thirteen droplets of inconsistent size are formed in the end. The snapshots at $t = 2$ present a thin connecting filament with small beads between the primary droplets, that is, the "beads-on-string" phenomenon appears, which is a well-known dynamical behavior of viscoelastic filament, see [40,42–44].

Third, we increase the elastic and anchoring constants to two more sets, i.e., $K = 4.2$, $\eta = 18$ that is shown in Fig. 4.5, and $K = 100$, $\eta = 20$ that is shown in Fig. 4.6. We observe the emergence of a lot of beads on strings. As long as the filament is pinched, tiny satellite droplets of different sizes appear on the thin string. In Fig. 4.7, we compare our simulation (part of $t = 1.2$ in Fig. 4.5) with the experimental photo in [40] side by side, where a good qualitative agreement can be seen.

4.3. Dripping LC droplet: "beads-on-string" phenomenon

In this numerical example, we simulate the dynamical motion of a dripping droplet under the action of gravity. We still set the computed domain $(r, z) \in \Omega$ to a cylinder with a radius of R and a height of L and assume that the

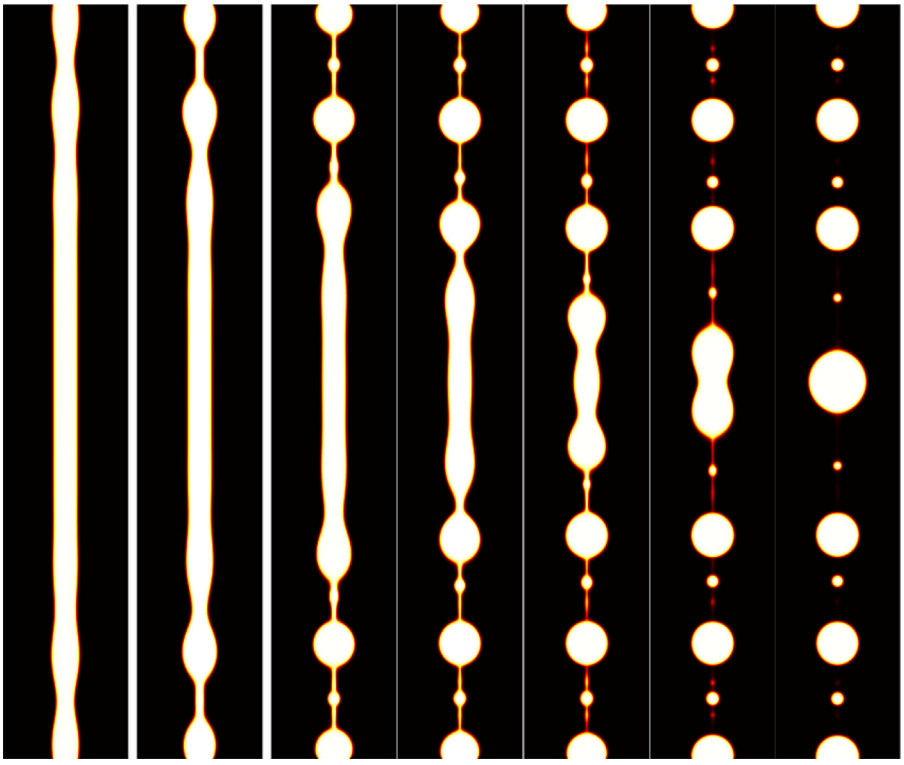

Fig. 4.5. The deformation of an axisymmetric LC filament that is immersed in another viscous fluid, where the elastic constant is $K = 4.2$ and the anchoring constant is $\eta = 18$. The snapshots are taken at $t = 0.6, 0.7, 0.8, 0.9, 1, 1.2, 1.4$.

problem is axisymmetric. The cylinder contains an immiscible mixture of viscous fluid and a cap-shape LC droplet (located on the top wall of the cylinder).

We assume the density difference between the droplet and the ambient fluid to be small, and use the so-called Boussinesq approximation to introduce the gravity to the fluid momentum equation (see [2,45]). Thus the fluid momentum equation (2.10) is replaced by

$$\mathbf{u}_t + (\mathbf{u}\cdot\nabla)\mathbf{u} - \nu\Delta\mathbf{u} + \nabla p = \boldsymbol{\omega}\nabla\mathbf{d} - \phi\nabla\mu + \nabla\cdot\sigma_e + (\rho_1 - \rho_2)\mathbf{g}_0\phi, \tag{4.5}$$

where $\mathbf{g}_0 = (0, g_0)$, g_0 is the gravity constant, ρ_1 is the density of the ambient fluid, and ρ_2 is the density of the lighter drop, see also the two-phase phase-field model with Boussinesq approximation in [46,47] and variable density/viscosity model in [45,48].

The initial conditions read as

$$\begin{cases} \phi^0(r,z) = \dfrac{1}{2}\tanh\left(\dfrac{R_0^2 - r^2 - (z - L - 0.6)^2}{\epsilon}\right) + \dfrac{1}{2}, \\ \mathbf{d}^0 = (0, \phi^0),\ \mathbf{u}^0 = (0,0),\ p^0 = 0. \end{cases} \tag{4.6}$$

The model parameters are set as follows,

$$\begin{cases} R = 1,\ L = 7,\ R_0 = 1.15,\ \rho_1 = 1,\ \rho_2 = 2,\ g_0 = 20,\ M_1 = 1\times10^{-3},\ \epsilon = 1.5\times10^{-2}, \\ \lambda = 0.1,\ B = 1,\ \phi_c = 1/2,\ s = 1.2,\ M_2 = 2\times10^{-3},\ \alpha = 5, \\ \nu = 1,\ \gamma = 1,\ S_\phi = 4/\epsilon^2,\ S_{\mathbf{d}} = 2,\ h = \dfrac{1}{256},\ \delta t = 1\times10^{-4}. \end{cases} \tag{4.7}$$

To show the effect of elastic energy on the drop dynamics, we first set the two parameters K and η very small, so that the elastic effect is very small and the filament is very close to the viscous fluid. Then we increase the elastic

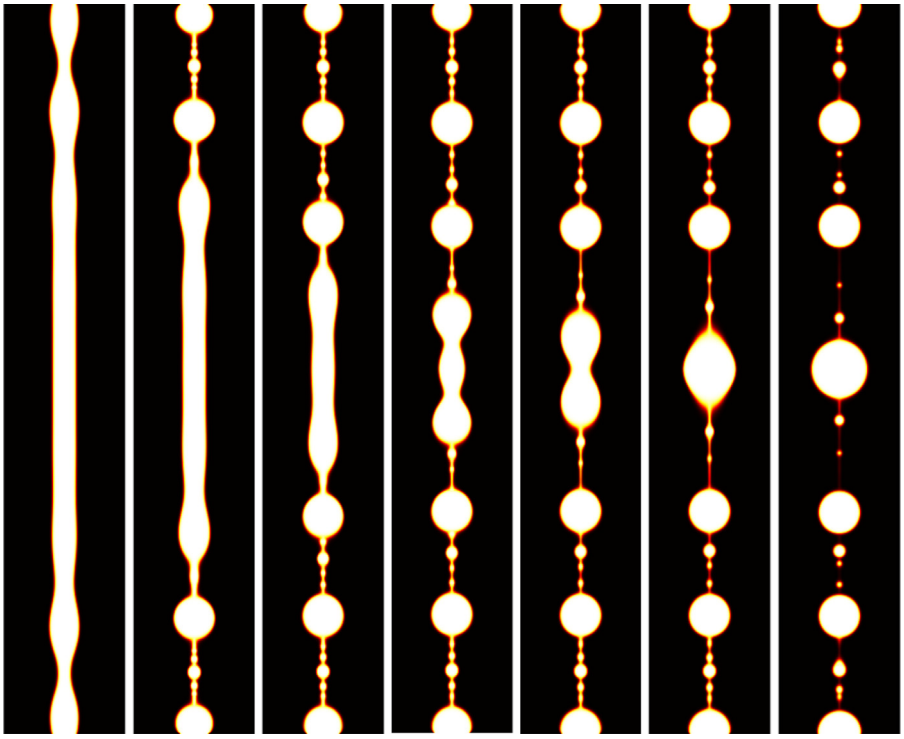

Fig. 4.6. The deformation of an axisymmetric LC filament that is immersed in another viscous fluid, where the elastic constant is $K = 100$ and the anchoring constant is $\eta = 20$. The snapshots are taken at $t = 0.2, 0.24, 0.28, 0.32, 0.35, 0.4, 0.44$.

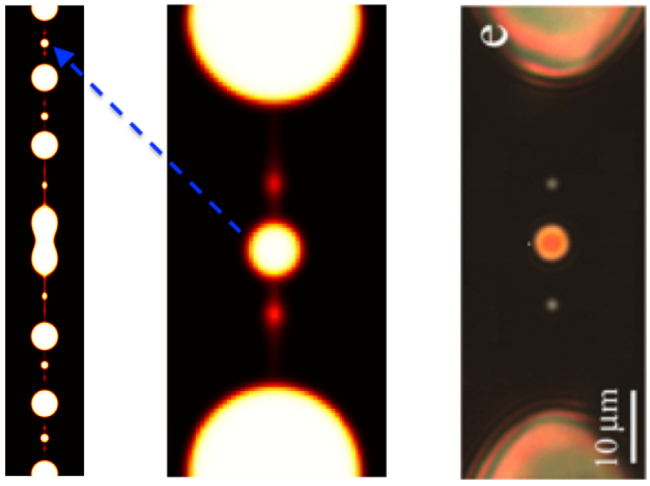

Fig. 4.7. Qualitative comparison of numerical simulation and experimental result. The three subfigures from left to right are, the snapshot at $t = 1.2$ in Fig. 4.5, the enlarged view of the top region, and the experimental photo given in [40] for nematic LC droplets.

constant K and the magnitude of the anchoring energy constant η to study the difference in the dripping dynamics of the LC droplet.

We simulate three different dripping situations of a droplet, (a) viscous droplet ($K = 1 \times 10^{-5}, \eta = 0$) (b) LC droplet with relatively weak elastic/anchoring parameters ($K = 30, \eta = 7$), and (c) LC droplet with relatively strong elastic/anchoring parameters ($K = 60, \eta = 14$). Fig. 4.8 gives the snapshots of the phase-field variable ϕ at various times for the viscous droplet. We observe that due to the action of gravity, the droplet slowly elongates

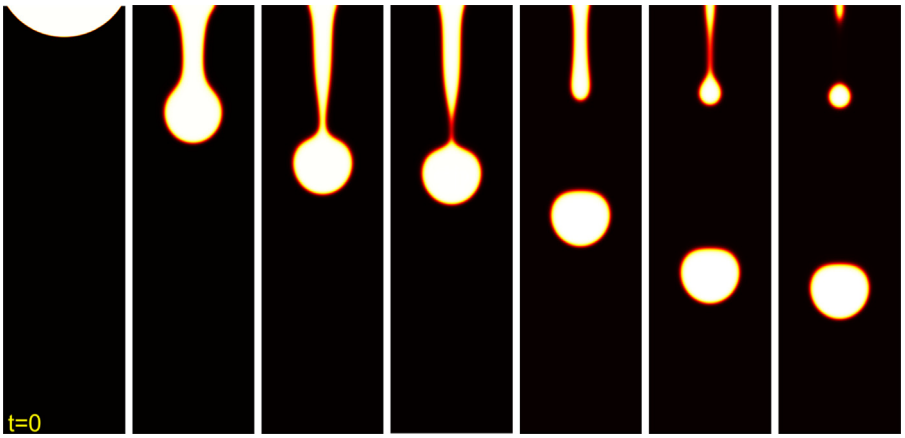

Fig. 4.8. The dripping dynamics of an axisymmetric viscous droplet that is immersed in another viscous fluid, where $K = 1 \times 10^{-5}$ and $\eta = 0$. Snapshots are taken at $t = 0, 1.5, 2, 2.1, 2.5, 3.05, 3.2$.

Fig. 4.9. The dripping dynamics of an axisymmetric LC droplet that is immersed in another viscous fluid, where $K = 30$ and $\eta = 7$. Snapshots are taken at $t = 0.25, 0.78, 1, 1.37, 1.4, 1.42, 1.45$.

Fig. 4.10. The dripping dynamics of an axisymmetric LC droplet that is immersed in another viscous fluid, where $K = 60$ and $\eta = 14$. Snapshots are taken at $t = 0.2, 0.4, 0.45, 0.475, 0.5, 0.525, 0.55$.

and becomes thinner. The lower end of the filament becomes a circular droplet under the action of capillary force. The falling droplet continues to stretch, causing the main droplet to be pinched off. After that, a similar process (filament stretching and pinching off) will occur, and a secondary satellite droplet is formed.

Fig. 4.9 depicts the dripping process of the LC droplet. It can be seen that, unlike the viscous droplet, the LC droplet exhibits the "beads-on-string" phenomenon. Due to the effect of gravity, the droplet stretches first and then forms a large circular droplet at the end. Between the head and tail of the two droplets, a very thin filament is formed, and a bead with a very small radius appears in the middle. Fig. 4.10 also exhibits the similar "beads-on-string" phenomenon, and due to very strong elastic/anchoring parameters, the thin filament carries more small beads. These simulations are qualitatively consistent with the experimental results given in [42].

5. Concluding remarks

In this article, we have established an efficient numerical scheme of the fully discrete version for the two-phase flow-coupled nematic-Newtonian model. The scheme contains many expected features, including second-order time accuracy, linearity, unconditional energy stability, and decoupling structure. The space is discretized by the finite element method, and the time is discretized by the newly developed explicit IEQ method. To realize unconditional energy stability and full decoupling calculation method, some auxiliary variables and their ODEs with specific forms are used to reformulate the system based on the "zero-energy-contribution" feature satisfied by the coupled nonlinear terms. The decoupling structure of the scheme enables independent calculation of all variables and each step only needs to solve a series of constant-coefficient elliptic equations independently. The detailed implementation, solvability, and rigorous proof of unconditional energy stability are also given. Numerous numerical examples are simulated, including the convergence and stability tests, as well as the benchmark "beads-on-string" phenomenon of LC filament/droplets to illustrate the effectiveness of the proposed scheme.

Declaration of competing interest

The authors declare that they have no known competing financial interests or personal relationships that could have appeared to influence the work reported in this paper.

Acknowledgments

The work of C. Chen was supported by the Shandong Province Natural Science Foundation with grant number No. ZR2021ZD03. The work of X. Yang was partially supported by the U.S. National Science Foundation under grant number DMS-2012490.

References

[1] J.J. Feng, X. Chen, P. Yue, C. Zhou. Chapter, 11, Drop Dynamics in Complex Fluids in the Book of Understanding Soft Condensed Matter Via Modeling and Computation, in: Series in Soft Condensed Matter - 3, 2010, pp. 339–363.
[2] P. Yue, J.J. Feng, C. Liu, J. Shen, A diffuse-interface method for simulating two-phase flows of complex fluids, J. Fluid Mech. 515 (2004) 293–317.
[3] R.L. Nós, A.M. Roma, C.J. García-Cervera, H.D. Ceniceros, Three-dimensional coarsening dynamics of a conserved, nematic liquid crystal-isotropic fluid mixture, J. Non-Newton. Fluid Mech. 248 (2017) 62–73.
[4] M. Mata, C.J. García-Cervera, H.D. Ceniceros, Ordering kinetics of a conserved binary mixture with a nematic liquid crystal component, J. Non-Newton. Fluid Mech. 212 (2014) 18–27.
[5] E. Tjhung, D. Marenduzzo, M.E. Cates, Spontaneous symmetry breaking in active droplets provides a generic route to motility, Proc. Natl. Acad. Sci. USA 109 (31) (2012) 12381–12386.
[6] J. Zhao, Q. Wang, X. Yang, Numerical approximations to a new phase field model for immiscible mixtures of nematic liquid crystals and viscous fluids, Comput. Methods Appl. Mech. Engrg. 310 (2016) 77–97.
[7] J. Huang, F. Lin, C. Wang, Regularity and existence of global solutions to the EricksenLeslie system in R^2, Comm. Math. Phys. 331 (2014) 805–850.
[8] F. Lin, C. Wang, Recent developments of analysis for hydrodynamic flow of nematic liquid crystals, Philos. Trans. R. Soc. Lond. Ser. A Math. Phys. Eng. Sci. 372 (2014) 20130361.
[9] H. Wu, X. Xu, C. Liu, Asymptotic behavior for a nematic liquid crystal model with different kinematic transport properties, Calc. Var. Partial Differential Equations 45 (2011) 319–345.
[10] F.C. Frank, On the theory of liquid crystals, Discuss. Faraday Soc. 25 (1958) 19–28.
[11] C. Zhou, P. Yue, J.J. Feng, Dynamic simulation of droplet interaction and self-assembly in a nematic liquid crystal, Langmuir 24 (2008) 3099–3110.

[12] J. Shen, X. Yang, Decoupled energy stable schemes for phase filed models of two phase complex fluids, SIAM J. Sci. Comput. 36 (2014) B122–B145.
[13] J. Zhao, X. Yang, J. Li, Q. Wang, Energy stable numerical schemes for a hydrodynamic model of nematic liquid crystals, SIAM. J. Sci. Comput. 38 (2016) A3264–A3290.
[14] J. Zhao, X. Yang, J. Shen, Q. Wang, A decoupled energy stable scheme for a hydrodynamic phase-field model of mixtures of nematic liquid crystals and viscous fluids, J. Comput. Phys. 305 (2016) 539–556.
[15] X. Yang, A novel fully-decoupled scheme with second-order time accuracy and unconditional energy stability for the Navier–Stokes equations coupled with mass-conserved Allen-Cahn phase-field model of two-phase incompressible flow, Internat. J. Numer. Methods Engrg. 122 (2021) 1283–1306.
[16] C. Chen, X. Yang, A second-order time accurate and fully-decoupled numerical scheme of the Darcy-Newtonian-nematic model for two-phase complex fluids confined in the Hele-Shaw cell, J. Comput. Phys. 456 (2022) 111026.
[17] X. Yang, On a novel fully-decoupled, linear and second-order accurate numerical scheme for the Cahn-Hilliard-Darcy system of two-phase hele-shaw flow, Comput. Phys. Comm. 263 (2021) 107868.
[18] X. Yang, A new efficient fully-decoupled and second-order time-accurate scheme for Cahn-Hilliard phase-field model of three-phase incompressible flow, Comput. Methods Appl. Mech. Engrg. 376 (2021) 13589.
[19] X. Yang, A novel fully-decoupled, second-order time-accurate, unconditionally energy stable scheme for a flow-coupled volume-conserved phase-field elastic bending energy model, J. Comput. Phys. 432 (2021) 110015.
[20] J.J. Feng, C. Liu, J. Shen, P. Yue, An energetic variational formulation with phase field methods for interfacial dynamics of complex fluids: advantages and challenges, IMA Vol. Math. Appl. 140 (2005) 1–26.
[21] J.L. Ericksen, Anisotropic fluids, Arch. Ration. Mech. Anal. 4 (1960) 231–237.
[22] F.M. Leslie, Some constitutive equations for anisotropic fluids, Q. J. Mech. Appl. Math. 19 (1966) 357–370.
[23] J.L. Ericksen, Liquid Crystals with Variable Degree of Orientation, in: IMA Preprint Series, 1989, p. 559.
[24] K. Kruse, J.F. Joanny, F. Julicher, J. Prost, K. Sekimoto, Asters, vortices, and rotating spirals in active gels of polar filaments, Phys. Rev. Lett. 92 (2004) 078101.
[25] P.G. de Gennes, J. Prost, The Physics of Liquid Crystals, Oxford University Press, 1993.
[26] S. Chandrasekhar, Liquid Crystals, Cambridge University Press, 1992.
[27] X. Feng, A. Prol, Numerical analysis of the allen-cahn equation and approximation for mean curvature flows, Numer. Math. 94 (2003) 33–65.
[28] J. Shen, X. Yang, Numerical approximations of Allen-Cahn and Cahn-Hilliard equations, Disc. Conti. Dyn. Sys.-A 28 (2010) 1669–1691.
[29] J. Shen, X. Yang, The IEQ and SAV approaches and their extensions for a class of highly nonlinear gradient flow systems, Contemp. Math. 754 (2020) 217–245.
[30] J. Shen, J. Xu, J. Yang, A new class of efficient and robust energy stable schemes for gradient flows, SIAM Rev. 61 (2019) 474–506.
[31] K. Cheng, C. Wang, S.M. Wise, An energy stable BDF2 Fourier pseudo-spectral numerical scheme for the square phase field crystal equation, Comm. Comput. Phys. 26 (2019) 1335–1364.
[32] V. Girault, P.A. Raviart, Finite Element Method for Navier-Stokes Equations: Theory and Algorithms, Springer-Verlag, Berlin, Heidelberg, 1987, pp. 395–414.
[33] J. Shen, On error estimates of the projection methods for the Navier-Stokes equations: second-order schemes, Math. Comp. 65 (215) (1996) 1039–1065.
[34] W. E., J.G. Liu, Projection method. I. Convergence and numerical boundary layers, SIAM J. Numer. 32 (1995) 1017–1057.
[35] W. Chen, Y. Liu, C. Wang, S. Wise, Convergence analysis of a fully discrete finite difference scheme for Cahn-Hilliard-Hele-Shaw equation, Math. Comp. 85 (2016) 2231–2257.
[36] Y. Liu, W. Chen, C. Wang, S. Wise, Error analysis of a mixed finite element method for a Cahn-Hilliard-Hele-Shaw system, Numer. Math. 135 (2017) 679–709.
[37] A. Diegel, C. Wang, X. Wang, S. Wise, Convergence analysis and error estimates for a second order accurate finite element method for the Cahn-Hilliard-Navier–Stokes system, Numer. Math. 137 (2017) 495–534.
[38] J. Guo, C. Wang, S. Wise, X. Yue, An improved error analysis for a second-order numerical scheme for the Cahn-Hilliard equation, J. Comput. Appl. Math. 388 (2021) 113300.
[39] K. Cheng, C. Wang, S. Wise, X. Yue, A second-order, weakly energy-stable pseudo-spectral scheme for the cahn-hilliard equation and its solution by the homogeneous linear iteration method, J. Sci. Comput. 69 (2016) 1083–1114.
[40] P.V. Dolganov, A.S. Zverev, K.D. Baklanova, V.K. Dolganov, Dynamics of capillary coalescence and breakup: Quasi-two-dimensional nematic and isotropic droplets, Phys. Rev. E 104 (2021) 014702.
[41] P.G. Drazin, W.H. Reid, Hydrodynamic Stability, Cambridge University Press, New York, 1981.
[42] V. Tirtaatmadja, G.H. McKinley, J.J. Cooper-White, Drop formation and breakup of low viscosity elastic fluids: Effects of molecular weight and concentration, Phys. Fluids 18 (2006) 043101.
[43] V. Cristini, Y.-C. Tan, Theory and numerical simulation of droplet dynamics in complex flows- A review, Lab Chip 4 (2004) 257–264.
[44] J. Eggers, Nonlinear dynamics and breakup of free-surface flows, Rev. Modern Phys. 69 (1997) 865–930.
[45] J. Shen, X. Yang, Decoupled, energy stable schemes for phase-field models of two-phase incompressible flows, SIAM J. Num. Anal. 53 (1) (2015) 279–296.
[46] C. Liu, J. Shen, A phase field model for the mixture of two incompressible fluids and its approximation by a Fourier-spectral method, Physica D 179 (3–4) (2003) 211–228.
[47] X. Yang, J.J. Feng, C. Liu, J. Shen, Numerical simulations of jet pinching-off and drop formation using an energetic variational phase-field method, J. Comput. Phys. 218 (2006) 417–428.
[48] H. Abels, H. Garcke, G. Grün, Thermodynamically consistent, frame indifferent diffuse interface models for incompressible two-phase flows with different densities, Math. Models Methods Appl. Sci. 22 (3) (2012) 1150013, 40.